UNIVERSITÀ
DEGLI STUDI
DI PADOVA

Università degli Studi di Padova

Dipartimento di Scienze chirurgiche oncologiche e gastroenterologiche - DISCOG

CORSO DI DOTTORATO DI RICERCA IN

ONCOLOGIA E ONCOLOGIA CHIRURGICA

-XXIX CICLO-

STUDY OF THE METABOLIC EFFECTS OF ANTI-ANGIOGENIC THERAPY IN EXPERIMENTAL MODELS OF OVARIAN CANCER

Coordinatore: Ch.ma Prof.ssa Paola Zanovello

Supervisore: Dott. Stefano Indraccolo

Dottoranda: Dott.ssa Carolina Venturoli

INDEX

RESULTS (2nd part)

4.10 Western blot analysis of silencing PDHK1 through lentiviral vectors

4.11 In vitro effects of silencing PDHK1 on cell proliferation

4.12 The effects of silencing PDHK1 on cell metabolism

4.13 In vivo effects of silencing PDHK1 on tumor growth

4.14 The effects of silencing PDHK1 on angiogenesis

4.15 Transcriptome analysis of shPDHK1 and shRNA in OVCAR3 model

4.16 Differentially regulated transcription factor targets in OVCAR3 shPDHK1 and shRNA

5. DISCUSSION

6. REFERENCES

ABSTRACT

In most of cancers, anti-angiogenic therapies are approved as a single-agent drug or in combination with cytotoxic chemotherapy. However, several works suggest that both in clinical and preclinical models, after an initial regression, tumors resume growth in the absence of active tumor angiogenesis.

Previous studies demonstrate that anti-angiogenic therapies perturb tumor metabolism toward anaerobic glycolysis and suggest that glycolysis inhibitors, such as 3PO or MCT4/MCT1 inhibitors, could be a new approach to overcome resistance after anti-angiogenic therapies, even if recent data are not so clear.

Furthermore, these results underline the importance to investigate better the metabolic changes, focusing on the intra-tumoral heterogeneity. Here, we demonstrate that *ex vivo* cultures derived from Bevacizumab treated tumors have marked metabolic heterogeneity, compared with control tumors. Starting from these evidences, we isolate and characterize clones with different glycolytic profiles. In particular, we speculated that highly glycolytic cells could be more glucose addicted and hence they less tolerate culture under glucose starvation. In order to identify different glycolytic subpopulations, that we call glucose deprivation resistant (GDR) or glucose deprivation sensitive (GDS) clones, we perform a glucose deprivation assay at different time points. Results demonstrate that GDR and GDS clones have transcriptomic and metabolomic differences. Therefore, investigation of the metabolic heterogeneity at clonal level could be a strategy to understand better the development of resistance to anti-angiogenic therapy and to find more efficient molecular targets.

1. INTRODUCTION

1.1 Cancer

Cancer is a major cause of mortality throughout the world and despite the extraordinary amount of work over the past decades, successful eradication and control of advanced disease remains elusive [1]. In parallel, our understanding of cancer biology and genetics has changed beyond recognition [2]. According to the International Agency for Research on Cancer (IARC), in 2012 there were 14.1 million new cancer cases and 8.2 million cancer deaths worldwide. By 2030, the global burden is expected to grow to 21.7 million new cancer cases and 13 million cancer deaths simply due to the growth and aging of the population. The future burden will probably be even larger because of the adoption of western lifestyles, such as smoking, fat rich diet and physical inactivity in economically developing countries [cancer.org, see references].

1.2 Hallmarks of cancer

The hallmarks of cancer, according to the original [3], comprise six biological capabilities acquired during the multistep development of human tumors. These hallmarks constitute an organizing principle for rationalizing the complexities of neoplastic disease. They include **sustaining proliferative signaling**, **evading growth suppressors**, **resisting cell death**, **enabling replicative immortality**, **inducing angiogenesis**, and **activating invasion and metastasis**. Underlying these hallmarks are **genome instability**, which generates the genetic diversity that expedites their acquisition, and **inflammation**, which fosters multiple hallmark functions. Conceptual progress in the last decade has added two emerging hallmarks of potential generality to this list; **reprogramming of energy metabolism** and **evading immune destruction**. In addition to cancer cells, tumors exhibit another dimension of complexity: they contain a repertoire of recruited, ostensibly normal cells that contribute to the acquisition of hallmark traits by creating the "tumor microenvironment." Recognition of the widespread applicability of these concepts will increasingly affect the development of new means to treat human cancer. Figure 1 shows all the hallmarks of cancer (old and the emerging) and drugs that interfere with each of the acquired capabilities necessary for tumor growth and progression. Some of these drugs are in clinical trials or in some cases are approved for clinical use in treating certain forms of human cancer. The drugs listed are illustrative

examples; there is a rich pipeline of candidate drugs with different molecular targets and modes of action in development for targeting most of these hallmarks [3].

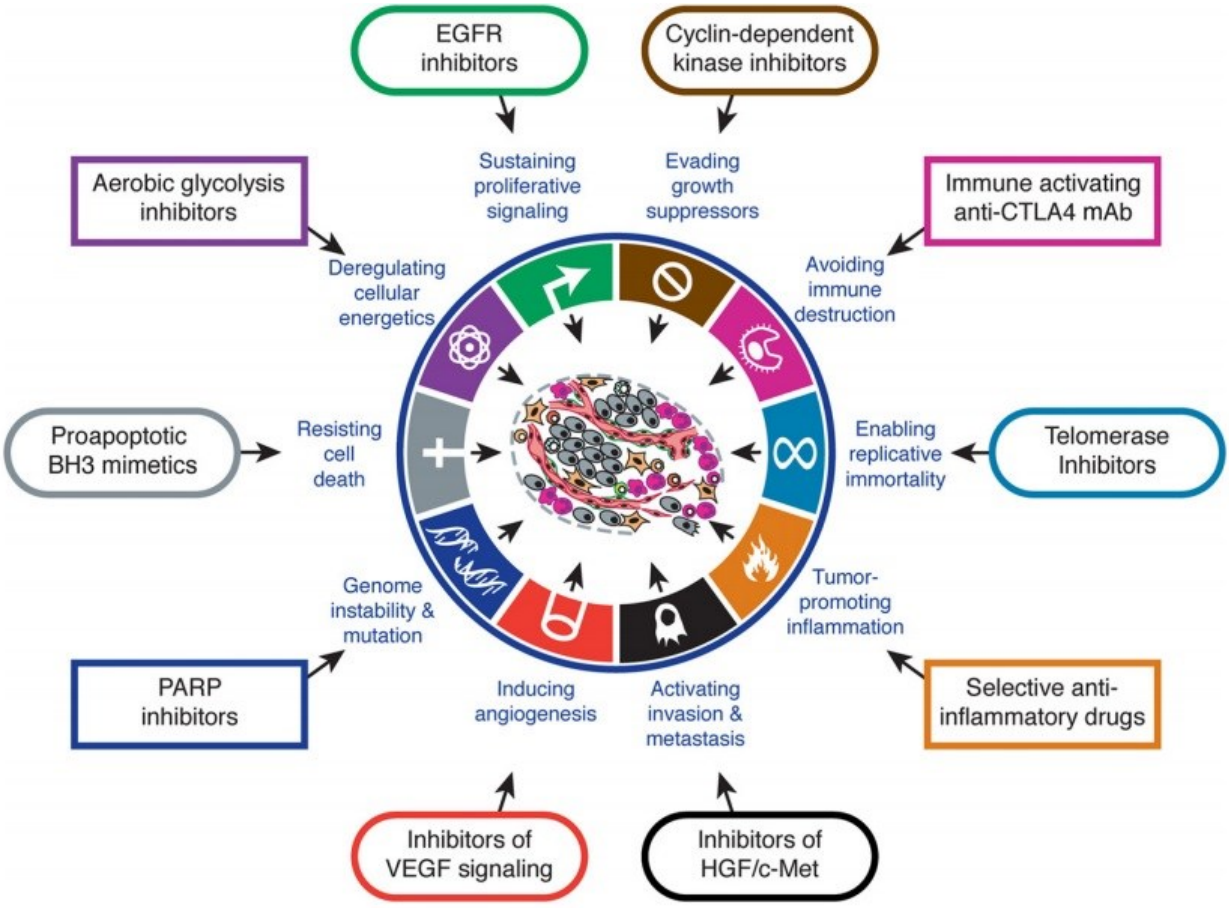

Figure 1

Schematic representation of therapeutic targeting of the Hallmarks of Cancer. The drugs listed are illustrative examples; there is a deep pipeline of candidate drugs with different molecular targets and modes of action in development for most of these hallmarks.

1.3 Ovarian cancer

Ovarian cancer is the fifth most common cancer in women and is most frequently in between 55-64 years. Survival rate varies greatly depending on the time of diagnosis, but approximately only 15 percent of ovarian cancer are diagnosed early with early stage disease. Although ovarian cancer has been termed the 'silent killer', more than 80% of patients have symptoms, even when the disease is still limited to the ovaries. However, symptoms are unspecific and shared with many more common gastrointestinal, genitourinary and gynecological diseases. Diagnosis can be formulated through transvaginal sonography (TVs) and serum markers, like the protein CA125. The combination of the two modalities could increase the percentage of disease detection at early stages (48%) with a sensitivity of 89,4% and a specificity of 99,8%. [4].

Ovarian cancer (represented in Figure 2) has a distinctive biology and behavior at the clinical, cellular and molecular levels. Some factors and conditions may increase a woman's risk of developing this cancer, like a family history of ovarian or breast cancer, germline mutations in BRCA1 and BRCA2 tumor suppressor genes. Most tumors of the ovary can be grouped into three major categories: epithelial, sexcord-stromal-, and germ cell tumors, according to the anatomic structures from which the tumors presumably originate. Each category includes a number of subtypes. Epithelial ovarian cancer is the most frequent form (95% of all the tumors); based on histopathology and molecular genetic alterations, it is divided into five subtypes: high-grade serous (70%), endometrioid (10%), clear cell (105%, mucinous (3%) and low-grade serous carcinomas (<5%).

The International Federation of Gynecology and Obstetrics (FIGO) has classified ovarian carcinoma in four stages [5] :

-Stage 1: tumor is confined to ovaries and Fallopian tubes;

-Stage 2: tumor involves one or both ovaries or Fallopian tubes with pelvic extension or primary peritoneal cancer;

-Stage 3: tumor involves one or both ovaries or primary peritoneal cancer, with cytologically or histologically confirmed spread to the peritoneum outside the pelvis and/or metastasis to the retroperitoneal lymph nodes;

- Stage 4: distant metastasis excluding peritoneal metastases.

Furthermore, one third of ovarian cancer patients presents with ascites, a generally voluminous exudative fluid with a cellular fraction consisting mainly of ovarian cancer cells, leucocytes and mesothelial cells.

1.3.1 Treatment of ovarian cancer

Treatment usually relies on surgery and chemotherapy, sometimes in combination with radiotherapy, and is obviously more efficient when the disease is confirmed to the ovary. Chemotherapy include the doublet carboplatin/paclitaxel as front line, followed by other cytotoxic drugs as the tumor relapses (such as liposomal doxorubicin, topotecan and gemcitabine). While patients with EOC initially respond to initial therapies, they often will become resistant to chemotherapy.

For this reason, ovarian carcinoma is considered a chemo-resistant cancer, and studying its biology to improve the outcome is mandatory [6].

Anti-angiogenic therapy is being considered for ovarian cancer and the European Medicines Agency (EMA) recently approved the use of the anti-VEGF antibody bevacizumab in patients with stage III and IV ovarian cancer, in combination with chemotherapy [7-9].

1.4 Angiogenesis

Angiogenesis is a tightly regulated biological process through which new blood vessels are generated from pre-existing ones. This is distinct from vasculogenesis, which is the *de novo* formation of endothelial cells from mesoderm cell precursors [10]. It occurs throughout life in both health and disease, beginning in utero and continuing on through old age. Angiogenesis is modulated by different factors that can either promote (pro-angiogenic) or inhibit (anti-angiogenic) this physiological process. Angiogenesis, in the context of cancer, plays an essential role in the formation of a new vascular network to supply nutrients, oxygen and bone marrow-derived cells to tumor cells. One of the most prominent proangiogenic molecules is vascular endothelial growth factor (VEGF) [11], also known as vascular permeability factor (VPF) because it efficiently potentiates permeabilization of blood vessels [12]. In mammals, there are five VEGF ligands, which occur in several splicing variants and processed forms and these ligands bind to specific receptors that exhibit a tyrosine-kinase activity (RTK). Biological effects of VEGF in endothelial cells are mainly regulated by three types of receptors, including VEGFR1, VEGFR2 and VEGFR3 [13]. Several studies showed that VEGF is implicated in the pathogenesis of ovarian cancer [14-16].

1.4.1 Anti-angiogenic therapies

Targeting angiogenesis might plausibly reduce intra-tumoral levels of oxygen and nutrients, resulting in tumor starvation and thus in reduced tumor growth [17]. Judah Folkman's vision of targeting the tumor neovasculature as a new modality of cancer therapeutics inspired the development of drugs that inhibit angiogenic signaling with different mechanisms of action [18, 19] with associated beneficial responses, representing proof of principle and new additions to the armamentarium of anti-cancer drugs. Anti-angiogenic therapies have been rapidly translated with great expectations from preclinical cancer models to clinical practice [20-23]. However, clinical responses to angiogenesis inhibitors (AI) are typically limited to improved progression-free survival with minor (or no) effects on overall survival. [24, 25]. Indeed, this has been reported in breast [26] and ovarian cancer patients [27], whereas better outcome, albeit without permanent disease stabilization, has been observed in renal cell carcinoma (RCC) [28, 29] and colorectal cancer (CRC) patients [30].

1.4.2 Mechanisms of resistance to anti-angiogenic therapies

Clinical investigations and different preclinical studies of AI in various mouse models of human cancer have revealed multiple forms of adaptive resistance that enable tumors to evade the effects of AI therapy [18, 24, 31-34] . These studies described several mechanisms of resistance to anti-angiogenic therapy. For example, Casanovas *et al.* reported that in renal cell carcinoma (RCC) models resistance to an antibody targeting VEGFR2 (MAb DC101) was due to hypoxia-triggered upregulation of other proangiogenic factors (FGFs and Ephrins) that stimulate tumor angiogenesis in a VEGF-independent manner. These findings suggested that treatments able to block both VEGF and FGF signaling could overcome this type of resistance.

Apart from this type of vascular resistance, resistance to anti-angiogenic drugs has also been associated with recruitment of certain subsets of bone marrow-derived cells or to selection of clones resistant to hypoxia, acquisition of an invasive phenotype, and overexpression of c-Met [24, 31, 35, 36].

Mechanisms of resistance to anti-angiogenic therapies not involving revascularization have been recognized more recently. For example, nintedanib- and sunitinib-resistant tumors do not show any evidence of revascularization. Rather, along with reduced tumor perfusion, hypoxia was increased in resistant tumors and microarray gene expression analysis revealed a metabolic shift to glycolysis in resistant tumors. Intra-tumor hypoxia induced by antiangiogenic factors produces an accumulation of tumor intrinsic and microenvironment modifications that enhance survival, including metabolic adaptations which enable tumor cells to survive under low oxygen (hypoxia) and low nutrient conditions [37, 38]. In this regard, glycolysis and glucose-transport-related genes are well known targets of hypoxia-induced cellular adaptations [39] and most metabolic pathways associated with hypoxia are involved in reprogramming of cancer cells [40].

One mechanism of resistance to anti-angiogenic therapy is associated with stable induction of the glycolytic phenotype [41, 42]. Curtarello *et al*., demonstrated that anti-VEGF therapy stably modulates the glycolytic phenotype in ovarian cancer models treated with bevacizumab, a recombinant humanized monoclonal IgG1 antibody that targets VEGF-A. The hypothetical mechanism behind this stable metabolic change could be represented by

either selection of a pre-existing subpopulation of highly glycolytic tumor cells or, alternatively, epigenetic reprogramming of cell metabolism.

Another particular form of adaptation to hypoxia is **metabolic symbiosis**, where there is a coordinated compartmentalization of tumor cells and their use of glucose and lactate. In severely hypoxic regions tumor cells import and metabolize glucose by anaerobic glycolysis with upregulation of glucose transporter GLUT1 and lactate transporter MCT4[43]. Hypoxic tumor cells depend on glucose and glycolysis to produce energy. Lactate, the end-product of glycolysis, diffuses along its concentration gradient toward blood vessels. By contrast, oxygenated tumor cells import lactate through MCT1 and oxidize it to produce energy. In the respiration process, lactate is a substrate preferred to glucose. As consequence, glucose freely diffuses through the oxygenated tumor cell sheath to fuel glycolysis of distant, hypoxic tumor cells. This metabolic symbiosis can be disrupted by MCT1 inhibition. Upon MCT1 inhibition, oxidative tumor cells switch from lactate oxidation to glycolysis, thereby preventing adequate glucose delivery to glycolytic cells, which die from glucose starvation. This glycolytic switch is associated with decrease in oxygen consumption of surviving tumor cells, which is responsible for increased tumor pO_2. For this reason, MCT1 inhibition is considered a possible antitumor strategy that indirectly eliminate hypoxic/ glycolytic tumor cells [44]. Recently, metabolic symbiosis has been described in several mouse models of cancer in response to potent angiogenesis inhibitors. Moreover, Allen *et al*. and Pisarsky *et al*. described possible strategies to overcome this type of resistance associated with antiangiogenic therapy but confirmatory studies in the clinical setting are still not available [45, 46]. The same authors anticipated that the metabolic shift triggered by anti-angiogenic therapy will represent a good target for glycolysis-targeting drugs. Indeed, combination therapy involving angiokinase inhibitors with 3PO, a glycolytic flux inhibitor, or with rapamycin, an mTOR and glycolysis inhibitor, was able to overcome resistance to anti-angiogenic treatment. However, pharmacological targeting of glycolysis in the context of anti-angiogenic therapy may be more complex than anticipated. Indeed, metabolomics analysis of tumor lysates from nintedanib-treated and control tumors failed to show any significant differences in central carbon metabolism between the two groups [46]. It was suggested that decoding relevant metabolic differences may be obscured by the concomitant presence of subpopulations with different metabolic profiles within the tumor samples. Therefore, improved tools to investigate metabolic heterogeneity are needed to develop appropriate therapeutic approaches targeting dysregulated metabolic features of cancer.

1.5 Metabolism and cancer

Metabolic reprogramming is considered an hallmark of cancer [3] and has received a substantial amount of interest over the past decade [47]. The first study which affirmed the role of metabolism in carcinogenesis is described by the German physiologist Otto Warburg, who in the 1920s, demonstrated that cancer cells - at variance with normal cells - rely on glycolysis instead of mitochondrial oxidative phosphorylation (OXPHOS) to produce ATP even under aerobic conditions [48]. Warburg originally hypothesized that the glycolytic switch in cancer cells was a consequence of defects in mitochondria, which impair aerobic respiration. Currently, however, it is known that mitochondria are generally not damaged in cancer cells, suggesting that aerobic glycolysis essentially represents an adaptive choice of tumours [49].

Glucose is a critical nutrient for proliferating cells, and it is used as primary substrate to generate ATP, as well as to synthesize amino acids, nucleotides, and fatty acids, and to regulate the redox potential so as to minimize the effects of reactive oxygen species (ROS) that damage cellular membranes and proteins [50, 51]. Aerobic glycolytic metabolism can provide sufficient energy for cell proliferation. The metabolism of glucose to lactate generates only 2 ATPs per molecule of glucose, whereas OXPHOS generates 36 ATPs upon complete oxidation of one glucose molecule. Another source of energy is glutamine, which is the second principal growth-supporting substrates contributes not only carbon but also the nitrogen required for biosynthesis of purine and pyrimidine nucleotides, glucosamine-6-phosphate, and nonessential amino acids [52, 53].

A variety of oncogenes have been shown to contribute to the metabolic adaptation of proliferating cells [54]. For instance, **C-MYC** increases expression of pyruvate dehydrogenase kinase 1 (PDHK1), the negative regulator of the pyruvate dehydrogenase (PDH), a gatekeeper enzyme that converts pyruvate into Acetyl-CoA. Furthermore, it increases expression of lactate dehydrogenase A (LDH-A), an enzyme which catalyzes the reductive conversion of pyruvate to lactate [55]. Finally, it upregulates MCT1, which facilitates efflux of lactate into the extracellular space [56].

Experimental evidence suggested that metabolic functions of **p53** may be essential for its role as a tumor suppressor, whereas other functions — including induction of cell- cycle arrest and apoptosis — are dispensable [57]. For example, TP53 maintains mitochondrial activity

through expression of cytochrome c oxidase 2, and loss of this gene recapitulates the metabolic consequences of the Warburg effect [57-59].

AKT regulates the expression of glucose transporters and enhances glucose capture by hexokinase II (HKII) and stimulates phosphofructokinase activity [54] . Moreover, AKT can also increase activity of hypoxia-inducible factor (HIF), thus further enhancing glycolysis [60] and PDHK1[61].
Mutations in *KRAS* or *BRAF* play important roles in regulating metabolic reprogramming in cancer, such as glucose and glutamine utilization, respectively [62, 63].

The therapeutic potential of targeting glycolysis has been under investigation, and several compounds have been clinically tested, but none has been approved [64]. Optimal use of these drugs will require a better understanding of cancer cell metabolism. It is also necessary to find effective and safe methods of administration and formulation of these drugs because it is important to remember that these drugs can also block glucose metabolism pathways in normal cells.

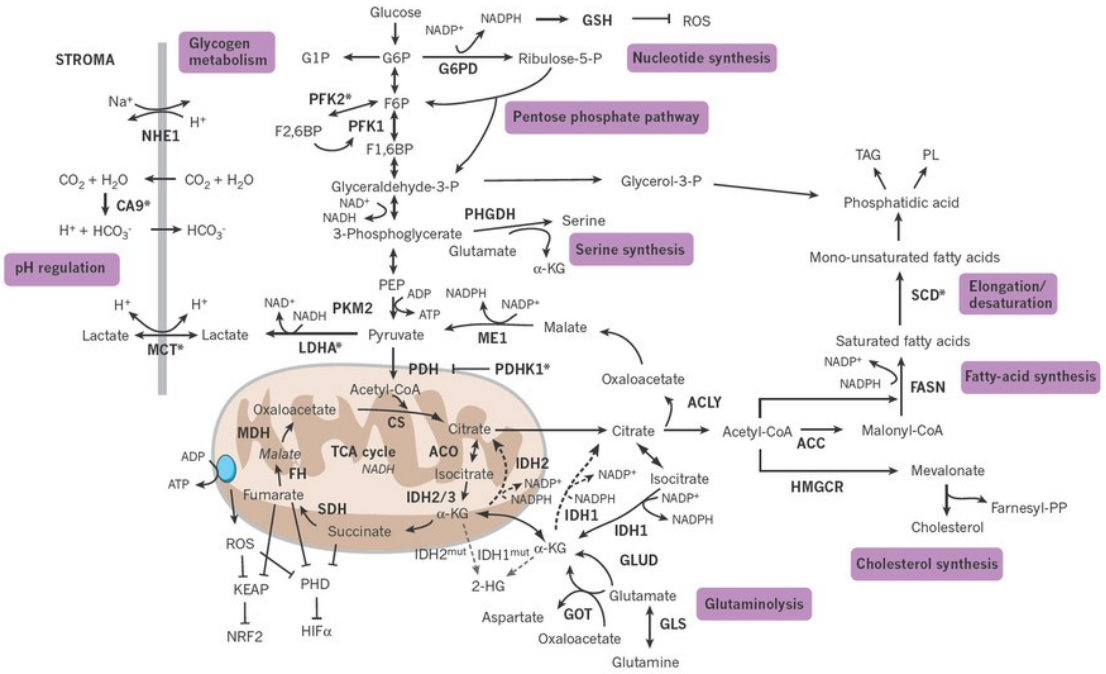

Figure 2

Overview of the main metabolic pathways in cancer cells (image from Nature, 2012.)

1.6 Metabolism and angiogenesis

Another interesting aspect is crosstalk between metabolism and angiogenesis. Elevated lactate concentrations represent an indicator of the metabolic adaptation of tumors and is actually correlated to clinical outcome in a variety of human cancers [65], [66]. Indeed, lactate modulate directly the endothelial phenotype and thereby tumor vascular morphogenesis and perfusion. It stimulates VEGF production by endothelial cells (EC), leading to enhanced migration and resulting in lactate-induced angiogenesis independently of O_2 conditions [67].

Végran *et al.* [68] demonstrated that lactate uptake in ECs through MCT-1 stimulates NF-κB activity and IL-8 expression. Furthermore, they showed that lactate release from tumor cells through MCT-4 is sufficient to stimulate IL-8–dependent angiogenesis and tumor growth in mice. A recent study reported a direct role of lactate in modulating angiogenesis independently of HIF. Lee et al. demonstrated that stabilisation of N-Myc downstream-regulated gene 3 (NDRG3) protein expression was associated with lactate-induced up-regulation of VEGF and IL-8, apparently via the ERK1/2 signalling pathway [69]. Tumor lactate levels predict metastases and overall survival of patients, as shown by several studies [70]. One of these demonstrated that increased extracellular lactate levels promote *in vitro* random migration of different cancer cells in a concentration-dependent manner, which could facilitate metastasis [71]. Sonveaux *et al*. showed that lactate increased EC motility and that MCT1 inhibition has anti-angiogenic effects [72]. Sutendra *et al.* observed pro-apoptotic, anti-proliferative and anti-angiogenic effects using dichloroacetate (DCA) - an inhibitor of pyruvate dehydrogenase kinase (PDK) - which functions by reverting the glycolytic cell phenotype to oxidative phosphorylation - in non-small cell lung cancer (nSCLC) models [73]. Also from our previous studies it can be inferred that poorly glycolytic cells - such as IGROV-1 ovarian cancer cell line - are less tumorigenic in mice compared to highly glycolytic cells - such as OC316 ovarian cancer cell line [42]. For these reasons, we consider it interesting to investigate the influence of metabolism on angiogenesis in cancer models.

1.7 Metabolic heterogeneity

Cancer occurs in a variety of taxonomically distinct species, characterized by divergent cells of origin and mutational spectra. Cancer cells acquire, via mutational and epigenetic changes, a variety of critical phenotype traits that compound to empower territorial expansion, via proliferative self-renewal, migration and invasion; properties that are part and parcel of normal developmental, physiological and repair processes [74]. Each cancer is individually unique and displays substantial intra-tumor heterogeneity in virtually all distinguishable phenotypic features, such as cellular morphology, gene expression, metabolism, motility, and angiogenic, proliferative, immunogenic, and metastatic potential.

In 1984, Gloria Heppner published *Tumor Heterogeneity*, a review in which the long-standing recognition that cancers are composed of multiple subpopulations was analyzed [75]. Some papers hypothesized that the cancer "stem cell" theory could explain the origins of heterogeneity [76-79]; others argued that genomic/genetic instability drives diversification of cancers [80-83]. Discussion about the heterogeneity of cancer often concerns the concept of clones [83].

1.7.1 The concept of clones

In 1976, Peter Nowell published a landmark perspective on cancer as evolutionary process driven by stepwise, somatic cell mutations with sequential, sub-clonal selection steps [84]. The implicit parallel was to Darwinian natural selection with cancer equivalent to an asexually reproducing, unicellular, quasi-species. The modern era of cancer biology and genomics has validated the fundamentals of cancer as a complex, Darwinian, adaptive system [85, 86].

Cancer can be viewed from an evolutionary perspective as a large, genetically and epigenetically heterogeneous population of individual cells. To understand cancer, it is important to understand and measure the population dynamics and evolutionary parameters of neoplasms [87]. Furthermore, recent works suggested that conventional therapies kill only some tumour cells, leaving behind therapeutically resistant clones and thus contribute to accelerate this evolutionary process.

In my PhD work, I focused on metabolic heterogeneity in ovarian cancer model, investigating sub-clones with different glycolytic profile to better understand the mechanism underling resistance to the anti-VEGF-therapy.

2. AIMS OF THE PhD THESIS

During my PhD, I focused on the correlation between tumor metabolism and anti-angiogenic therapy. First of all, I studied the metabolic heterogeneity at clonal level to better understand the mechanisms associated with resistance to anti-angiogenic therapy in ovarian cancer models. Second, I investigated effects of silencing of the pyruvate dehydrogenase kinase (PDHK1) on tumor metabolism and angiogenesis.

2.1 FIRST AIM

Previous studies from our and other laboratories demonstrated that anti-VEGF therapy stably modulates the glycolytic phenotype of tumor xenografts and that such metabolic rewiring correlates with tumor aggressiveness and resistance to anti-angiogenic therapy (M. Curtarello, 2015; E. Allen, 2016; L. Pisarsky, 2016). These studies, however, did not investigate the possible existence of metabolic heterogeneity in tumor samples treated with this anti-angiogenic drug. Starting from the idea that the clonal heterogeneity could play a fundamental role to study the effects of anti-angiogenic therapy, we tried to isolate and characterize clones with different metabolic profiles from ex vivo cultures of EOC xenografts. Moreover, we studied the transcriptomic and metabolomic differences between glucose deprivation resistant (GDR) and glucose deprivation sensitive (GDS) clones. Finally, we characterized these two subpopulations in order to find molecular targets that could help to overcome resistance to anti-VEGF therapy.

2.2 SECOND AIM

We investigated the potential connection between the glycolytic phenotype of cancer cells and their tumorigenic and angiogenic potential. We focused on pyruvate dehydrogenase kinase 1 (PDHK1), an enzyme that sits at key bifurcation point between glycolysis and OXPHOS. For this purpose, we silenced PDHK1 expression by lentiviral vectors in two different highly glycolytic ovarian cancer cell lines (OC316 and OVCAR3). We studied the proliferative and

metabolic effects of the inactivation of PDHK1 *in vitro* as well as *in vivo*. Moreover, we investigated effects of modulation of glycolysis by PDHK1 silencing on tumour angiogenesis.

3. MATERIALS AND METHODS

3.1 Cell lines and *in vitro* culture conditions

In this work, we used different cancer cell lines:

- IGROV-1, that were purchased from ATCC
- OC316 cells were provided by S. Ferrini (IST, Genoa, Italy)
- OVCAR3 and SKOV-3 cells were kindly provided by S. Canevari (INT, Milan, Italy).

All ovarian cancer cell lines were cultured in RPMI 1640 (EuroClone, Milan, Italy) supplemented with 10% (for OVCAR3 it was used 20%) FCS (Fetal Bovine Serum, Life technologies, Paisley, UK), 10mM HEPES (Cambrex Bioscience, East Rutherford, NJ), 1% Sodium Pyruvate, 2 mM L-glutamine and 1% of antibiotic-antimycotic mix (Life Technologies). The human embryonic kidney epithelium cell line 293T was purchased from ATCC and cultured in Dulbecco modified Eagle medium (Euroclone), supplemented with 10% FCS, 10 mM HEPES and 1% of antibiotic-antimycotic mix (Life Technologies, Paisley, UK). At the indicated time points, cells were harvested and processed for assessment of cell viability, and RNA and protein extraction. The cultures were routinely maintained at 37°C in a humidified 5% CO_2/95% air atmosphere.

3.2 Measurement of glucose and lactate

Cells ($2x10^5$) were plated in 6-wells tissue culture plates and incubated, in order to allow adhesion. After 48 hours supernatants were collected, centrifuged for 10 minutes for 3000g and then analysed. Glucose and lactate concentrations in supernatants were determined by colorimetric methods on an automated analyzer (Dimension RxL, Dade Behring, Milan, Italy). Values were normalized to cell numbers at the end of the incubation period.

3.3 Seahorse analysis: Oxygen Consumption and Extracellular Acidification Rate

The Seahorse XF24 Extracellular Flux Analyzer (Seahorse Bioscience, San Jose, CA) is an instrument that measures two parameters: **O**xygen **C**onsumption **R**ate (OCR) and Extracellular ACidification Rate (ECAR).

Cells (2.5 x10^4) were plated in 5 replicates in RPMI medium supplemented with 10% FBS. The following day, cells were placed in running DMEM medium (supplemented with 25 mmol/L D-glucose, 2 mmol/L glutamine, 1 mmol/L sodium pyruvate, and without serum and bicarbonate) and preincubated for 30 minutes at 37°C in atmospheric CO_2 before starting metabolic measurements.

The cartridge of the instrument was loaded to dispense four different metabolic inhibitors at 20 min intervals: olygomycin (1μM), followed by carbonyl cyanide *p* trifluoromethoxyphenylhydrazone, FCCP (0.4 μM), antimycin (1μM) and rotenone (1μM; all from Sigma Aldrich) over 2h. Some analysis to measure only the ECAR were performed initially depriving glucose to cells and after adding glucose, oligomycin, 2-deoxyglucose (2-DG) and finally the medium. This analysis was performed to confirm and reinforce basic results.

At the end of the experiment, OCR and ECAR values were normalized for the protein content of each sample. Accurate titration with the uncoupler FCCP was performed for each cell type, to utilize an FCCP concentration (400 nmol/L) that maximally increases OCR without being toxic.

3.4 Sulforhodamine B assay

The sulforhodamine (SRB) assay is used for cell content determination, based on the measurement of the amount of cellular proteins in a 96-well format. After an incubation period, cell monolayers are fixed with 10% (wt/vol) trichloroacetic acid and stained for 30 minutes, after which the excess dye is removed by washing repeatedly with 1% (vol/vol) acetic acid. The protein-bound dye is dissolved in 10 mM Tris base solution for OD determination at 510 nm using a microplate reader.

3.5 Flow cytometry

3.5.1 Annexin-V Apoptosis assay

To evaluate effects of glucose starvation on cell proliferation**,** $2x10^5$ cells per well were plated in 6-wells tissue culture plates and incubated, in order to allow adhesion. The following day, the medium was changed. Cell viability was evaluated following 48 hours of deprivation of glucose, using Annexin V/PI Staining Kit (Roche Applied Sciences; Penzberg, Germany). Cells were stained with 2 µl Annexin-V Fluos, 2 µl propidium iodide and 100 µl Hepes buffer, according to the manufacturer's instruction. Following an incubation of 15 minutes in the dark, staining was blocked with 200 µl Hepes buffer and results were expressed as cell viability, considering the percentage of Annexin V^-/PI^- cells at the experimental time point.

3.5.2 PKH26 Staining

To evaluate cell proliferation, cells were stained with the fluorescent dye PKH26 (Sigma Aldrich, St. Louis, MO) which is a lipophilic membrane binding dye that irreversibly binds to lipid regions of the cell membrane. Labeling was performed using a final PKH26 concentration of 4µL in 2 ml of Buffer C for $3x10^6$ cells. After 3 min incubation with the dye, staining was blocked with 2 ml of 1% BSA + 4 ml of RPM1 and centrifugated for two times and finally seeded in 6 wells in RPM1 at $1x10^5$/well. Cells labeled with PKH 26 retain the dye for a long time and during each cell division pass it down to daughter cells with a proportional reduction in the intensity of the dye in each cell.

3.5.3 Evaluation of GLUT1, MCT4 expression and glucose uptake

To evaluate glucose uptake, cells were labelled with 2-NBGD-FITC glucose (12.5 µM; Invitrogen) and fluorescence intensity measured after 5, 30 and 120 minutes. To determine the glycolytic capacity cells were used the antibody anti-MCT4 (1.1000; Santa Cruz) and anti-GLUT1 (1:1,000; Abcam). Intracellular staining was performed after fixation with 4% paraformaldeyde and permeabilization with 0.1% Triton X-100. After incubation with unconjugated antibodies, cells were incubated for 30 minutes with the appropriate secondary antibody (Alexa 1:500; Invitrogen).

All the cytofluorimetric analyses were performed using a FACS LSRII (BD Bioscience, Franklin Lakes, NJ); data were collected from at least $1x10^5$ cells/sample and elaborated with

FlowJo software (TreeStar, Ashland, OR). Glucose uptake was evaluated in parallel by confocal microscopy

For FACS-sorting, antibody-labelled cells were separated with a MoFlo Astrios Cell Sorter (Beckman Coulter, Brea, CA).

3.6 Generation of clones

To generate clones, 96-well plates were seeded with nominal 0.5-4 cells per well in 100 ul tissue culture medium and incubated at 37°C 5% CO_2. Two-three weeks later, 10-20 clones were obtained from each culture (generally from plates seeded with 0.5-1 cells/well) and further expanded for functional studies.
To identify glucose deprivation sensitive (GDS) and glucose deprivation resistant (GDR) clones, clones were split into two wells and incubated for 48-72 h either in the presence or in the absence of glucose (2 g/l). Scoring of clones and assessment of their GDS/GDR behaviour was done under an inverted microscope (Leika).

3.7 Metabolomic analysis

3.7.1 Metabolomic samples preparation

GDS and GDR clones, derived from IGROV-1 *ex vivo* cultures derived from Bevacizumab-treated tumor or Control, respectively were seeded at $1x10^6$ cells in Petri dishes in a total volume of 10 mL in biological replicates (n = 3 for) for each clone. Forty-eight or seventy-two hours after seeding, all clones were in exponential growth with quite same proliferation rate. After a period of incubation at 37° C, cells were washed two times with PBS and one wash with H_2O milli Q. Then, we poured 10 mL liquid nitrogen into the plates for some seconds and when it evaporated, plates were sealed and stored them at −80 °C until metabolomic analysis.

3.7.2 Direct Flow Injection-TOF MS/MS

In collaboration with Dott. Roberta Pastorelli and Dott. Laura Brunelli (Mario Negri Institute, Milan), clones were extracted and analyzed within seven days from freezing. Extraction was done by adding 1mL of ice-cold MeOH H2O (85:15) to each plate and cells were scraped.

Extracts were transferred to 1.5mL micro-centrifuge tubes and pelleted at 4 °C for 15min at 10000×g. Supernatants were stored at −80 °C. Twenty µL of each supernatant were used for untargeted metabolomics analysis.

The analysis was performed on an Agilent 1290 infinity Series coupled to an Agilent 6550 iFunnel Q-TOF mass spectrometer (Agilent, Santa Clara, CA) equipped with an electrospray source operated in negative and positive mode. The flow rate was 150 µL/min of mobile phase consisting of isopropanol/water (60:40, v/v) buffered with 5 mM ammonium at pH 9 for negative mode and methanol/water (60:40, v/v) with 0.1% formic acid at pH 3 for positive mode. Reference masses for internal calibration were used in continuous infusion during the analysis (m/z 121.050873, 922.009798 for positive and m/z 11.9856, 1033.9881 for negative ionization). Mass spectra were recorded from m/z 50 to 1100. Source temperature was set to 320 C with 15 L/min drying gas and a nebulizer pressure of 35 psig. Fragmentor, skimmer, and octopole voltages were set to 175, 65, and 750 V, respectively. MS/MS fragmentation pattern of the significantly features were collected and used to confirmed metabolite identity.

3.7.3 Data Processing and Metabolite identification

All steps of data processing and analysis were performed with Matlab (The Mathworks, Natick) using in-house developed pipeline. Briefly, in this procedure, we applied a cutoff to filter peaks of less than 500 ion counts for negative and 1000 ion counts positive ionization ion counts to avoid detection of background features. Centroid m/z lists from different samples were merged to a single matrix by binning the accurate centroid masses within the tolerance given by the instrument resolution (about 20 ppm). The resulting matrix lists the intensity of each mass peak in each analyzed sample. Because mass axis calibration is applied online during acquisition, no m/z correction was applied during processing to correct for potential drifts. Singular metabolic species were identified by database searches (METLIN, http://metlin.scripps.edu; HMBD, http://www.hmdb.ca/; in positive and negative ionization.

3.8 RNA extraction, reverse transcription PCR (RT-PCR), quantitative RT-PCR (qRT-PCR)

Total RNA was extracted from cells using Trizol® reagent (Life Technologies), according to the manufacturer's instruction. RNA concentration was determined using NanoDrop ND-1000 Spectrophotometer (NanoDrop Technologies Inc, Wilmington, DE). The instrument provided the sample concentration in ng/μl and the absorbance of the sample at 260nm and 280nm. The ratio (260/280) ranging from 1.8 to 2.1 indicated good quality of RNA (ratio < 1.8 means protein contamination and ratio > 2.1 RNA degradation and truncated transcripts).

cDNA was synthesized from 1 μg of total RNA using the "High Capacity RNA-to-cDNA™ Kit"(Applied Biosystems). Reverse transcription was followed by quantitative PCR using SYBR Green. mRNA PCRs were performed in an ABI Prism 7900HT Sequence Detection System. All reagents were obtained from Life Technologies. Results were analysed using the ΔΔCt method with normalization against β2-microglobulin expression. Primers used for q RT-PCR analysis were:

PDHK1 forward: 5'-AAGTTCATGTCACGCTGGGT-3'

PDHK1 reverse: 5'-CGAGGTCTTGGTGCAGTTGA-3'

GLUT1 forward: 5'-GATGATGCGGGAGAAGAAGG-3'

GLUT1 reverse: 5'-AAGACAGCGTTGATGCCAGAC-3'

B2M forward: 5'-TGCTGTCTCCATGTTTGATGTATCT-3'

B2M reverse: 5'-TCTCTGCTCCCCACCTCTAAGT-3'

HKII forward: 5'-GAAGATGCTGCCCACCTTTG-3'

HKII reverse: 5'-CACCCAAAGCACACGGAAGT-3'

3.9 GeneChip Analysis

RNA quality and purity control was assessed with the Agilent Bioanalyzed 2100 (Agilent Technologies, Waldbronn, Germany) using "Eukaryote total RNA Assay". To perform gene expression experiments only RNA samples with RIN >6 were used. Only RNA samples that passed the quality controls (RIN>6) were diluted to 100 ng in a total volume of 3 μL DEPC treated water. It was used the **GeneChip® WT PLUS Reagent Kit HTA** to investigate the transcriptome of clones (GDR and GDS) and **GeneChip® 3' IVT PLUS Reagent Kit**

(Primeviews) to analyze the transcriptome of the shRNA and shPDHK1 deficient OVCAR3 tumors.

The Affymetrix GeneChip Scanner was used to measure all intensities of the signals of each probe set on the GeneChip and stores all signals in a .DAT file (Raw image). Integrated software converts all raw signals into numbers, which were stored in a .CEL file. All GEP profiles used in these experiments were assessed for their comparability and quality by using different quality controls: Scale Factor, number of present calls, internal probe calls, Poly-A controls and the ratio GAPDH/β-actin 3'/5'.

Differential expression analysis was executed by using Expression Console (Affymetrix) and Affymetrix® Transcriptome Analysis Console (TAC) Software. Gene Set Enrichment Analysis (GSEA) was performed to evaluate the functional significance of curated sets of genes. Genes were ranked by log-FC and GSEA pre-ranked was run with default parameters, using gene set collections from the Molecular Signatures Database v5.2 (http://www.broadinstitute.org/gsea/msigdb/index.jsp). Specifically, we tested the significance of KEGG and Biocarta pathways, present in the "c2.cp.kegg" and "c2.cp.biocarta" collections and tested the significance of 615 gene sets that contain transcription factor targets (TFT), as defined in the "c3.tft" collection.

3.10 Western Blot analysis

Cells were resuspended in lysis buffer (NP-40 1%, NaCl 150 mM, Tris HCl pH7.5 50 mM, EDTA 2mM, NaF, Na_3VO_4 and protease inhibitor cocktail) and lysates obtained were quantified using Quantum protein Assay (Euroclone). Thirty μg of proteins were denaturated and loaded in a midi polyacrylamide gel 4-12% (Life Tecnologies). Separated proteins were transferred for 2 h at 400mA on a nitrocellulose membrane (GE Health Care, Glattbrugg, Switzerland)**.** Membranes were saturated for 1 hour with PBS - 0,1% Tween - 5% - milk and then incubated over night with primary antibodies at 4°, according to manufacturer's instructions.

In this work, the following primary antibodies were used:

- Mouse anti-TUBULIN (Sigma Aldrich);
- Rabbit anti-PDHK1 (Cell Signalling, Danvers, MA);
- Rabbit anti-GLS1 (Abcam, Cambridge, UK);
- Rabbit LC3 (Cell Signaling, Danvers, MA)

- Rabbit p-CREB (Cell Signaling, Danvers, MA)
- Rabbit CREB (Cell Signaling, Danvers, MA)

Membranes were washed two times for 15 minutes and incubated for 1 hour with horseradish-conjugated secondary antibodies (Amersham-Pharmacia; Little Chalfont, UK). Detection was obtained using Western Lightning plus ECL reagents (PerkinElmer), containing Luminol, which is oxidized by horseradish peroxidase, resulting in light emission at 425 nm. Signals emitted were acquired using ChemiDoc™ XRS system (Bio-Rad; Hercules, CA, USA.

3.11 Lentiviral vector-mediated transduction of shRNA in ovarian cancer cells

Lentiviral vectors were generated using 293T cells, due to their high transfection capacity. The lentiviral plasmids containing PDHK1 shRNA expression cassette or an unrelevant shRNA sequence were purchased from Sigma-Aldrich. The lentiviral vectors were produced as previously described [88]. Cells expressing the different shRNA were selected in puromycin-containing medium for 10-14 days prior to subsequent analysis.

3.12 Animals and treatments

Xenografts were generated by subcutaneously (s.c) injecting 0.3×10^6 to 0.5×10^6 different ovarian tumor cells mixed at 4°C with liquid Matrigel (Becton-Dickinson) into both dorsolateral flanks of severe combined immunodeficient (SCID) mice (Charles River). To study the metabolic heterogeneity as a mechanism of resistance after anti-VEGF therapy we used Anti-human VEGF monoclonal antibody (mAb; A4.6.1, Bevacizumab) that was administered intraperitoneally (i.p.) at 100 μg/dose every 2 days, and mice were sacrificed 48 hours after the last treatment. Control mice received i.p. injections of PBS. To study the relationship between glycolysis and angiogenesis silencing PDHK1 we injected subcutaneously $0.3x10^6$ shRNA or shPDHK1 cells into both flanks and after about two months animals were sacrificed and the tumor mass was cut and processed.

Tumor volume (mm^3) was measured by a caliper and calculated according to the following formula: $L \times l^2 \times 0.5$, where L is the longest diameter, l is the shortest diameter, and 0.5 is a constant to calculate the volume of an ellipsoid. Procedures involving animals and their care were performed according to institutional guidelines that comply with national and

international laws and policies (EEC Council Directive 86/609, OJ L 358, 12 December, 1987).

3.13 Immunohistochemistry analysis (IHC)

Quantification of necrosis was carried out by calculating the percentage of the necrotic area in the entire tumor section by using a light microscope equipped with digital camera and MODEL software (Leica Microsystems, Wetzlar, Germany). For immunohistochemical analysis, 5 μm-thick paraffin-embedded tumor sections were re-hydrated and then antigen retrieval was performed by incubation with citrate buffer 0.01M pH 6.0 at 95°C for 20 min. To evaluate proliferation, after saturation with 5% pre-immune serum, slides were incubated with rabbit anti-p-HH3 (#9701, Cell Signaling, Beverly, MA), according to the manufacturer's instructions. Slides were subsequently washed and incubated with the appropriate secondary Ab. Immunostaining was performed using the avidin-biotin-peroxidase complex technique (Vectastain ABC kit, Vector Labs, Burlingame, CA) and 3-3' diaminobenzidine (DAB kit, Dako) was used as chromogen substrate. Finally, tumor sections were counterstained with Mayer's hematoxylin. Specificity of each staining procedure was confirmed by replacing the primary Ab with PBS. Immuno-reactivity was scored semi-quantitatively for both the intensity and the proportion of cells staining: intensity was given scores 0-3 (no staining = 0; light staining = 1; moderate staining = 2; strong staining = 3) and proportion was given scores 1-6 (0-4% = 1; 5-20% = 2; 21-40% = 3; 41-60% = 4; 61-80% = 5; 81-100% = 6). The two scores were multiplied to obtain the final result of 0-18. The percentage of positive tumors was calculated and graphed as average and SD in each treatment group. Mann–Whitney statistical test or t test was used to determine significance $P < 0.05$.

Tumor vessels were labelled with rat anti-CD31 mAb (1:50 dilution; cat. 550274; BD Pharmingen, Franklin Lakes, NJ) followed by staining with a goat anti-rat 546 secondary antibody (Invitrogen, Milan, Italy) and quantification of microvessel density (MVD) as detailed elsewhere [89]. Scoring was performed by an experienced biologist at our Institution.

3.14 Statistical analysis

Results were expressed as mean value ± SD. Statistical analysis of data was performed using Student's t-test or Mann-Whitney test. Differences were considered statistically significant when $P \leq 0.05$.

4. RESULTS

4.1 VEGF-targeted therapy stably modulates the glycolytic phenotype of ovarian cancer cells

Previous studies from our and other laboratories demonstrated that anti-VEGF therapy (Bevacizumab) stably modulates the glycolytic phenotype of tumor cells in epithelial ovarian cancer (EOC) xenografts, and that such metabolic rewiring correlates with tumor aggressiveness and resistance to anti-angiogenic therapy (M. Curtarello, 2015; E. Allen, 2016; L. Pisarsky, 2016). These studies, however, did not investigate the possible existence of metabolic heterogeneity in tumor samples treated with this antiangiogenic drug.

To obtain new tumor samples to investigate this phenomenon, we set up an *in vivo* experiment with the IGROV-1 model. Following establishment of subcutaneous tumor xenografts, mice were treated with two or three weekly administrations of Bevacizumab for 4 weeks. Figure 1A shows that in tumors treated with Bevacizumab there is an initial response, lasting about 2 weeks, followed by slight increase in tumor volume, which indicates emergence of secondary resistance to anti-VEGF therapy. Immuno-histochemical analysis of tumor samples obtained at sacrifice showed persisting reduction of $CD31^+$ blood micro-vessels in tumors treated with Bevacizumab (Figure 1B), indicating was this type of resistance was not due to bypassing the anti-angiogenic effect of Bevacizumab by up-regulation of other pro-angiogenic factors in the tumor. Moreover, in agreement with previously published data, we observed a slight but significant increased expression of several glycolysis associated transcripts, including HKII, PDHK1 and GLUT1, in Bevacizumab-treated compared to Control tumors (Figure 1C). Furthermore, *ex vivo* cultures established from anti-VEGF-treated IGROV-1 tumors had significantly higher glucose consumption and lactate production rates, compared with cultures from control tumors (Figure 1D-E), along with increased cell death under glucose starvation (data not shown), suggesting selection of glucose-addicted tumor cells. Surprisingly, however, despite these metabolic differences, transcriptome analysis failed to disclose differentially expressed transcripts between cultures established from control and Bevacizumab-treated tumors (data not shown).

To try to explain this finding, we observed that individual cultures established from Bevacizumab-treated tumors (BEVA) had marked metabolic heterogeneity, compared with control cultures (CTRL) (Figure 1D-E): some *ex vivo* cultures, such as BEVA2 and BEVA6, had markedly aberrant values of lactate production and corresponding glucose consumption, compared with control cultures, whereas other cultures, including BEVA3 and BEVA4,

behave in this assay similarly to control cultures, and finally other cultures, including BEVA1, BEVA5, and BEVA7, had intermediate levels of metabolic variation compared with controls. To better characterize this heterogeneity, we focused on two BEVA cultures with marked or intermediate metabolic deviations, compared with control tumors. We also included in the analysis two control cultures representative of a poorly glycolytic phenotype (CTRL9) or an average control sample (CTRL12). By Seahorse analysis, we found increased ECAR in both BEVA cultures compared with CTRL cultures; in contrast, OCR levels were markedly reduced in BEVA6 but not in BEVA5 culture, compared with CTRL cultures (Figure 1F-G). To investigate whether these metabolic alterations were affecting the tumorigenic potential of these cells, we injected both BEVA5, 6 and CTRL9, 12 cells in the subcutaneous tissue of SCID mice. Results, shown in Figure 1H, indicated increased tumor growth by the more glycolytic cells (BEVA5 and BEVA6), compared to control cells.

These observations brought to our attention the phenomenon of metabolic heterogeneity, which is particularly exacerbated among tumors treated with Bevacizumab. This phenomenon can severely hamper attempts to further characterize the stable metabolic and molecular changes caused by this anti-VEGF drug in tumor cells, and prompted us to develop novel strategies to enrich for metabolically homogeneous samples for subsequent analysis.

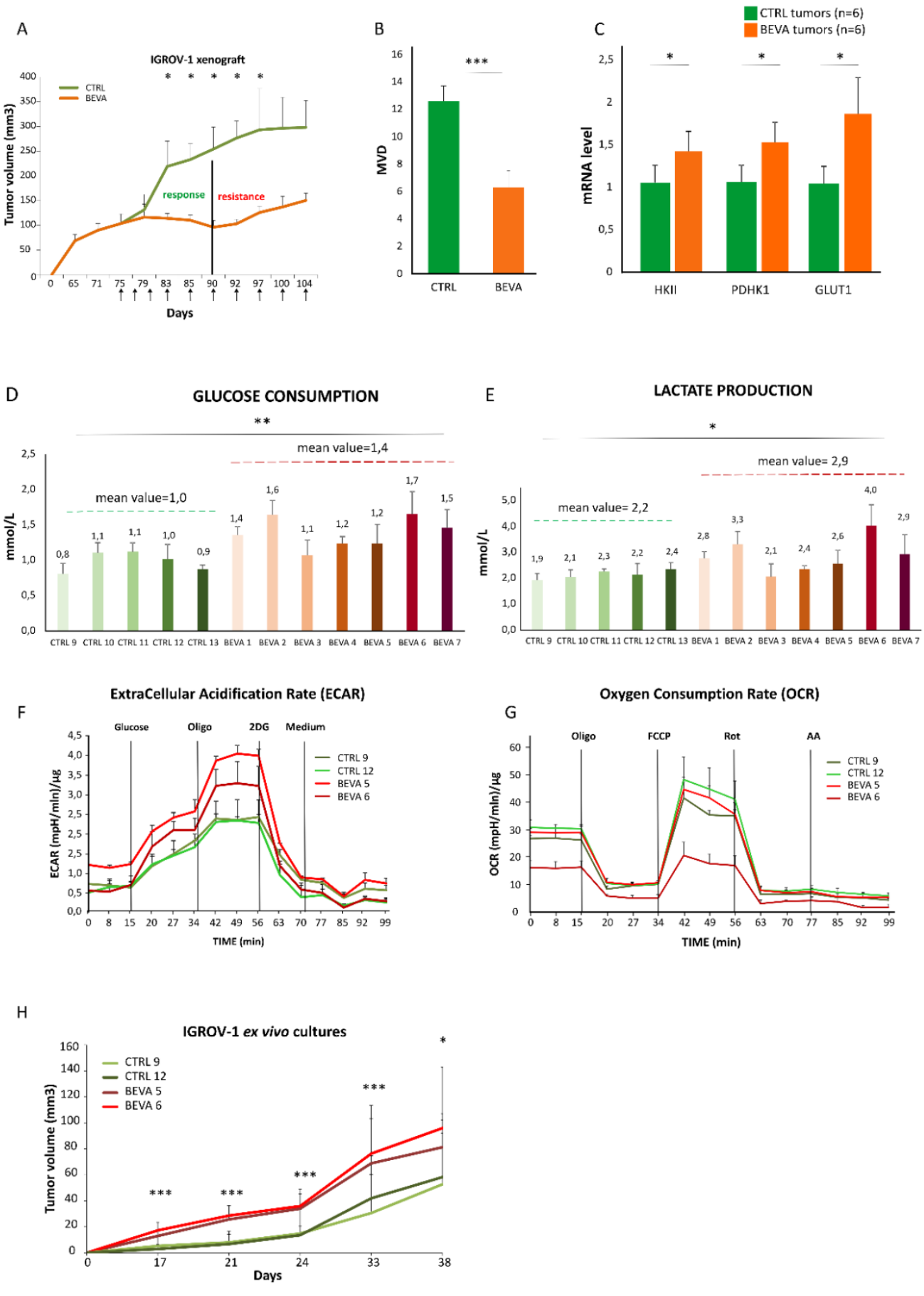
A
IGROV-1 xenograft
CTRL
BEVA
Tumor volume (mm3)
response
resistance
Days
B
MVD
CTRL
BEVA
C
CTRL tumors (n=6)
BEVA tumors (n=6)
mRNA level
HKII
PDHK1
GLUT1
D
GLUCOSE CONSUMPTION
mean value=1,0
mean value=1,4
mmol/L
CTRL 9 CTRL 10 CTRL 11 CTRL 12 CTRL 13 BEVA 1 BEVA 2 BEVA 3 BEVA 4 BEVA 5 BEVA 6 BEVA 7
E
LACTATE PRODUCTION
mean value= 2,2
mean value= 2,9
mmol/L
CTRL 9 CTRL 10 CTRL 11 CTRL 12 CTRL 13 BEVA 1 BEVA 2 BEVA 3 BEVA 4 BEVA 5 BEVA 6 BEVA 7
F
ExtraCellular Acidification Rate (ECAR)
Glucose
Oligo
2DG
Medium
ECAR (mpH/min)/µg
CTRL 9
CTRL 12
BEVA 5
BEVA 6
TIME (min)
G
Oxygen Consumption Rate (OCR)
Oligo
FCCP
Rot
AA
OCR (mpH/min)/µg
CTRL 9
CTRL 12
BEVA 5
BEVA 6
TIME (min)
H
IGROV-1 ex vivo cultures
CTRL 9
CTRL 12
BEVA 5
BEVA 6
Tumor volume (mm3)
Days

Figure 1: Metabolic heterogeneity following anti-VEGF therapy

A. Kinetics of tumor development in SCID mice subcutaneously injected with IGROV-1 tumor cells and effects of multiple injections of the anti-VEGF mAb Bevacizumab (arrows, 100 mg/dose administered bi- or triweekly) on tumor size compared with the size of controls (n=7 mice for group). *p < 0.05, t test. Tumors were collected and analyzed two days after the last dose of anti-VEGF mAb or PBS for Bevacizumab and control groups, respectively.

B. Vascularization of tumors by staining with anti-CD31 mAb and calculation of MVD. Columns show mean ± SD values (n= 5–10 fields per tumor; n= 6 tumors per group), *** p < 0.001, t test.

C. qRT-PCR analysis of glycolytic associated genes in tumor samples. Columns show mean values ± SD (n=6 samples per group).

D, E. Measurement of glucose consumption and lactic acid production by *ex vivo* cultures of IGROV-1 cells established from IGROV-1 tumors untreated (CTRL) or treated for 28 days with anti-VEGF therapy (BEVA). Average volumes of control and Bevacizumab tumors at sacrifice were 298,15 mm^3 and 150,16 mm^3, respectively. *Ex vivo* cultures were maintained in flasks up to 10 to 15 days before analysis. Cells were plated in P6 wells at 2x 10^6 cells/well, incubated for 48 hours *in vitro* under normoxic conditions, and metabolic parameters were quantified by an automated analyzer. Columns represent the mean value of three replicates for each sample. Over the dotted line the mean value of five samples for control group (green) and seven samples for the bevacizumab group (orange) is shown.). *p < 0.05, **p<0.01, t test.

F, G. Bio-energetic analysis of *ex vivo* cultures of IGROV-1 tumors. Measurement of OCR and ECAR traces obtained from two *ex vivo* cultures obtained from untreated mouse xenografts (CTRL 9 and 12) and two *ex vivo* cultures derived to treated tumors with anti-VEGF mAb (BEVA 5 and 6). The first three measurements of ECAR were obtained in glucose deprivation condition and then glucose was added to medium (the next three measurements). Subsequent additions of Oligomycin (ATP synthase inhibitor), of the 2-deoxyglucose (2DG) and finally of the medium were carried out. OCR measurements were performed in separated F12-wells. Subsequent additions of Oligomycin (ATP synthase inhibitor), of FCCP (uncoupler), of Rotenone (the ETC complex I inhibitor), and of Antimycin A (respiratory complex III inhibitor) were carried out. Data are mean ± SD values of ten replicates normalized to protein content. The experiment was assessed in all *ex vivo* cultures and results show the existence of a heterogeneity.

H. Kinetics of tumor development following subcutaneous injection of well characterized *ex vivo* cultures derived from IGROV-1 control tumors (CTRL 9 and 12, green lines) and *ex vivo* cultures derived from anti-VEGF-treated IGROV-1 tumors (BEVA 5 and 6, red lines). Eight SCID mice for each group were injected with 4x10^5 cells in both flanks. *p<0.05, ***p<0.001, t test.

4.2 How to study metabolic heterogeneity?

To study metabolic heterogeneity it was necessary to find a marker or a screening assay to isolate cell subpopulations endowed with different glycolytic activity. Initially, we analyzed by flow cytometry expression of surface markers associated with glycolysis, including the glucose transporter GLUT1 and the lactate transporter MCT4. Results, however, failed to disclose any significant difference in the expression levels of these markers between BEVA and CTRL cultures, (Figure 2A-B). In the case of GLUT1, a trend towards increased expression in BEVA cultures was found, but overall expression levels of this marker were quite low (range 2-16%), discouraging its use as bait to sort highly glycolytic cells by FACS. As alternative strategy, we monitored glucose uptake of glucose by using 2-[*N*-(7-nitrobenz-2-oxa-1,3-diazol-4-yl)amino]-2-deoxy-D-glucose (2-NBDG), a fluorescent analogue of glucose which is imported into the cells by GLUTs and subsequently is not further metabolized. Fluorescence measurements were performed at different time points (5, 30, and 120 minutes) following incubation of the cells with this tracer. We used IGROV-1 and OC316 cell lines as negative and positive control, respectively. Results showed that *ex vivo* CTRL cultures accumulated 2-NBDG much more avidly compared to *ex vivo* BEVA cultures, particularly at the 2 h time point (Figure 2C). Confocal microscopy confirmed these results (Figure 2D). Intrigued by these findings, we investigated the possibility to sort 2-NBDG-labelled cells from CTRL12 *ex vivo* culture, which showed relatively good uptake of the tracer (Figure 2C). Starting from 1 million of cells, we obtained $1.5x10^5$ 2-NBDG$^+$ and about $2x10^5$ 2-NBDG$^-$ cells. Seven to ten days later, following expansion of sorted cells in culture, we reanalyzed them and found that although relative enrichment in 2-NBDG$^+$ or NBDG$^-$ cells was maintained, each FACS-sorted subpopulation contained a quote of cells with the complementary 2-NBDG phenotype, which represented up to 30% of the total population (Figure 2D). Due to the relatively unstable 2-NBDG phenotype, we decided to focus on another strategy to obtain tumor cell populations with different glycolytic phenotype, which will be explained in the next paragraph.

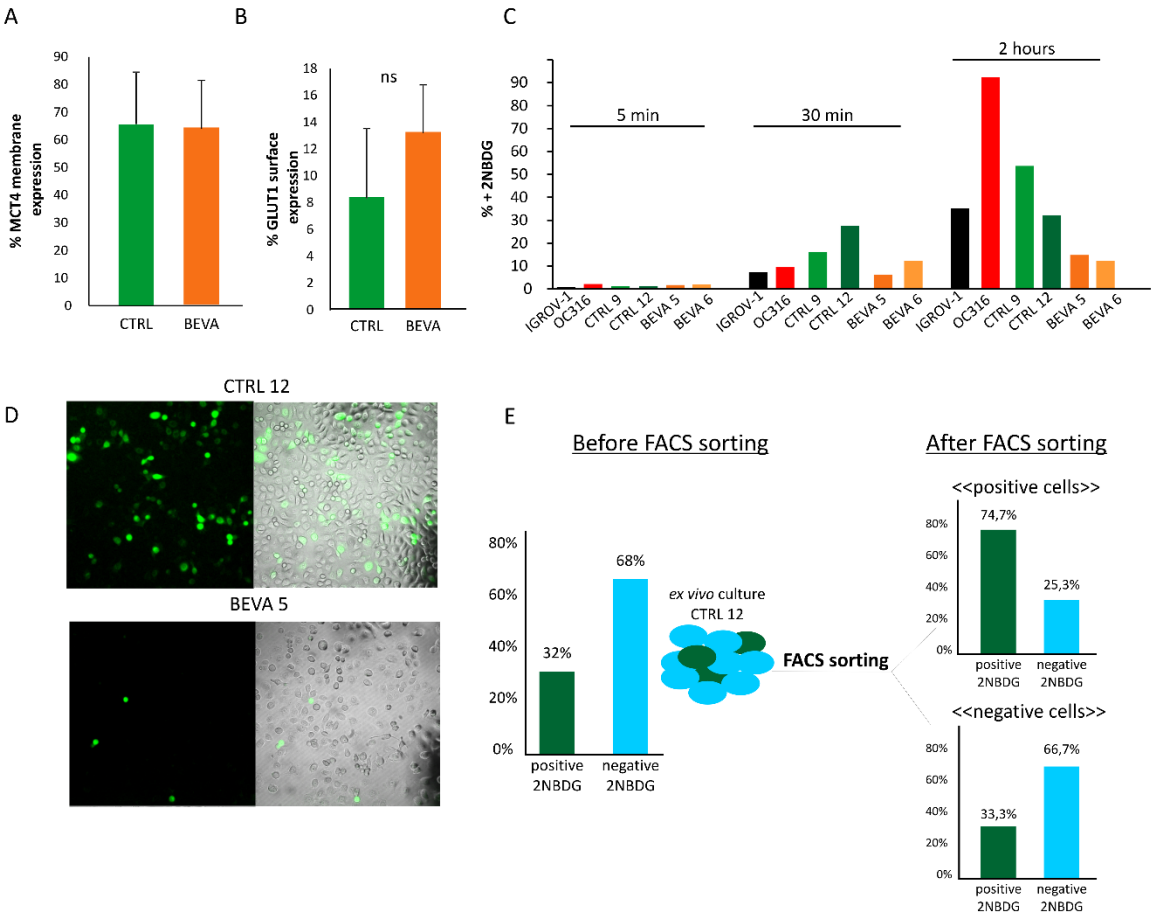

Figure 2

A. Flow cytometry analysis of the membrane expression of the lactate transporter MCT4 evaluated in five *ex vivo* cultures derived from Control tumors (green histogram) and five *ex vivo* cultures derived from Bevacizumab tumors (orange histogram). **B**. Surface expression of the glucose transporter GLUT1 evaluated by flow cytometry in five *ex vivo* cultures derived from Control tumors and five *ex vivo* cultures derived from Bevacizumab tumors. **C**. Flow cytometry analysis of fluorescent glucose uptake by 2NBDG staining in two *ex vivo* cultures obtained from mouse xenografts untreated (CTRL 9 and 12, green histograms) and two *ex vivo* cultures derived from Bevacizumab treated tumors (BEVA 5 and 6, orange histograms). The fluorescence intensity of 2NBDG was recorded after 5, 30 minutes and two hours of incubation. IGROV-1 (black histogram) and OC316 (red histograms) cell lines were used as negative and positive controls. **D**. Representative confocal pictures of glucose uptake by 2NBDG staining after 2 hours of incubation in CTRL 12 and BEVA 5 *ex vivo* cultures. **E**. Sorting experimental layout of the *ex vivo* culture derived from CTRL 12 culture as a potential strategy to isolate highly and poorly glycolytic subpopulations. In the left panel, it is represented the percentage of 2NBDG positive or negative cells in CTRL 12 before the FACS sorting. Then, 2NBDG positive or negative cells were isolated by FACS-sorting. Cells were kept in culture for two weeks. In the right panel, it is represented the percentage of the positive and negative cells re-analyzed by FACS after the culture step.

4.3 Identification and characterization of clones with different survival under glucose starvation

We speculated that highly glycolytic cells could be more glucose addicted and hence less tolerate culture under glucose starvation. To test this hypothesis in metabolically well characterized cells, we initially isolated clones from IGROV-1 and OC316 cells, which are a prototype of poorly and highly glycolytic cells, respectively. By seeding cells at extremely low numbers per well (typically, 4, 2, 1, 0.5 cells/well) through serial dilutions, we obtained several clones from each cell line analyzed. Subsequently, clones were split and cultivated in P96 wells either in the presence (2 G/L) or in the absence of glucose (0 G/L) in the medium for 72 h (Figure 3A-C). In this phase, by daily observations of the clones under the microscope, we evaluated their level of glucose addiction. We used the acronym GDS to refer to a Glucose Deprivation Sensitive clone or GDR to indicate a clone relatively resistant to glucose deprivation (Figure 3D-E). We analysed n=20 and n=35 clones from IGROV-1 and OC316 cell lines, respectively (Figure 3F) and various clones (range n=8-38) from each *ex vivo* culture of IGROV-1 tumors (Figure 3G). Analysis of the GDS/GDR proportions in OC316 and IGROV-1 cells disclosed that OC316-derived clones were exclusively of the GDS type, whereas in the case of IGROV-1-derived clones 55% and 45% had the GDR and GDS profile, respectively (Figure 3F). In the case of CTRL tumor-derived samples (n=109), we found 53% and 47% GDR and GDS clones, a proportion which is similar to that found in the parental cells, never passaged in vivo. In the case of BEVA tumor-derived clones (n=89), we found 63% and 37% GDR and GDS clones, respectively. In this latter group, however, there were several samples which contained an excess of GDR clones, such as in the case of BEVA1, BEVA2 and BEVA7 cultures and only one culture had an excess of GDS clones, which is BEVA5 (Figure 3G), suggesting that, there is an increase of the GDR amount, although no statistically significant if compared to CTRL clones was found. To this study, we were interested in the subpopulation derived from Bevacizumab group more glucose addicted.

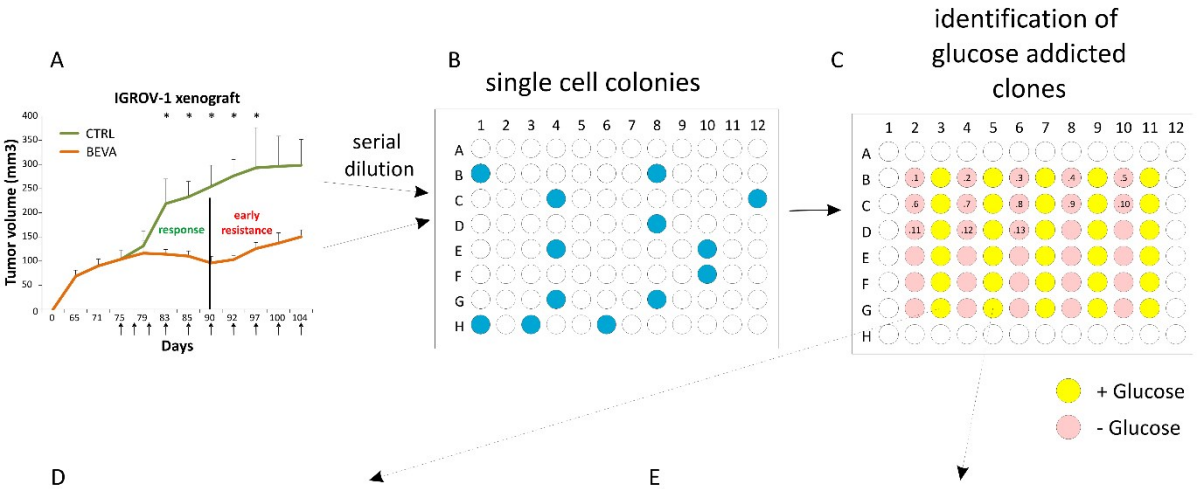

D

GDR=Glucose Deprivation Resistant

+glucose

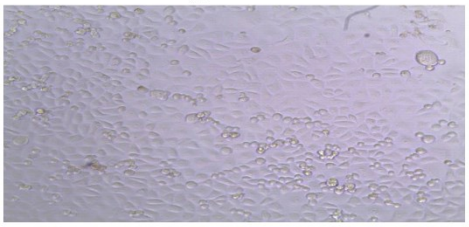

- glucose

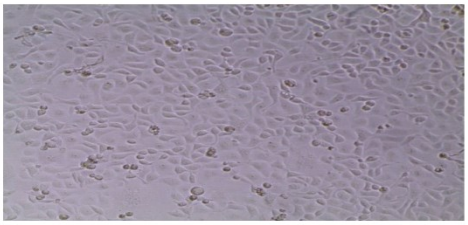

E

GDS= Glucose Deprivation Sensitive

+ glucose

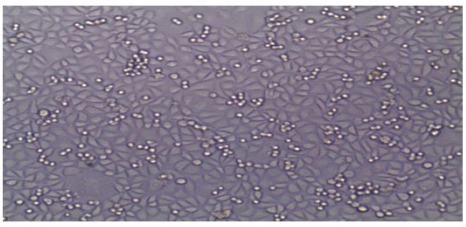

- glucose

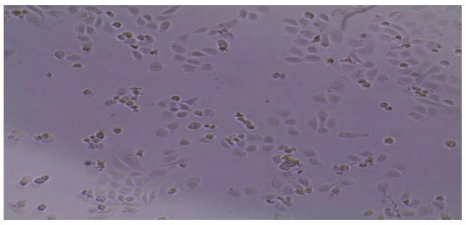

F

	TOTAL CLONES	GDR	GDS	%GDR	%GDS
IGROV-1	20	11	9	55%	45%
OC316	35	0	35	0%	100%

G

	TOTAL CLONES	GDR	GDS	%GDR	%GDS
CTRL 9	8	4	4	50%	50%
CTRL 10	38	18	20	47%	52%
CTRL 11	32	18	14	56%	44%
CTRL 12	15	11	4	44%	56%
CTRL 13	16	7	9	44%	56%
BEVA 1	11	11	0	100%	0%
BEVA 2	31	19	12	61%	39%
BEVA 5	10	1	9	8%	92%
BEVA 6	14	8	6	57%	43%
BEVA 7	23	17	6	74%	26%

Figure 3

Experimental layout: isolation of clones from IGROV1 and OC316 cell lines (not shown in the figure) and then isolation of clones from *ex vivo* cultures (n=8-38/*ex vivo* culture) by limiting dilution analysis (**A**). **B**. Representative image of recognition of clones originated by each cell lines or/and *ex vivo* cultures. **C**. Representative image of identification of glucose deprivation sensitive (GDS) or glucose deprivation resistant (GDR) clones by cultivating clones for 48-72 h either in the presence or the absence of glucose in the medium. Scoring of the clones was done by optical microscopy. **D**. Representative pictures showed that GDR clones are vital both in presence (up) or in absence (down) of glucose. **E**. Representative images showed that GDS clones are vital in presence of glucose (up) but are suffering in absence of glucose. **F**. Summary table of clones originated by IGROV-1 and OC316 cell lines. **G**. Summery table of clones originated by *ex vivo* cultures (CTRL or BEVA).

4.4 Selection GDS and GDR clones for transcriptome and metabolomics analysis

To investigate which molecular and metabolic hallmarks could distinguish these two types of clones, we performed gene expression profiling and targeted metabolomics analysis of n=5 GDS clones from the BEVA 5 culture, which was highly enriched in GDS clones, and compared results with those obtained in clones derived from CTRL 12, which contained a mix of GDS/GDR clones. We confirmed our initial observations through a cell viability assay upon glucose starvation at 72 hours, which showed that GDS clones were more sensitive to glucose deprivation compared to GDR ones (Figure 4A). We further investigated the glycolytic profile of these clones by other techniques prior to "omics" analysis. Initially, we measured surface expression of GLUT1 by flow cytometry analysis, but we did not find any significant correlation between the expression of GLUT1 and the GDR and GDS phenotype, although it unexpectedly emerged that CTRL clones had much higher sGLUT-1 expression levels than BEVA clones (Figure 4B-C). Furthermore, we analyzed by q-PCR expression of one of the most important enzyme associated with glycolysis, hexokinase II (HKII). As panel D shows, GDS clones expressed slightly more HKII transcript, compared to GDR clones.

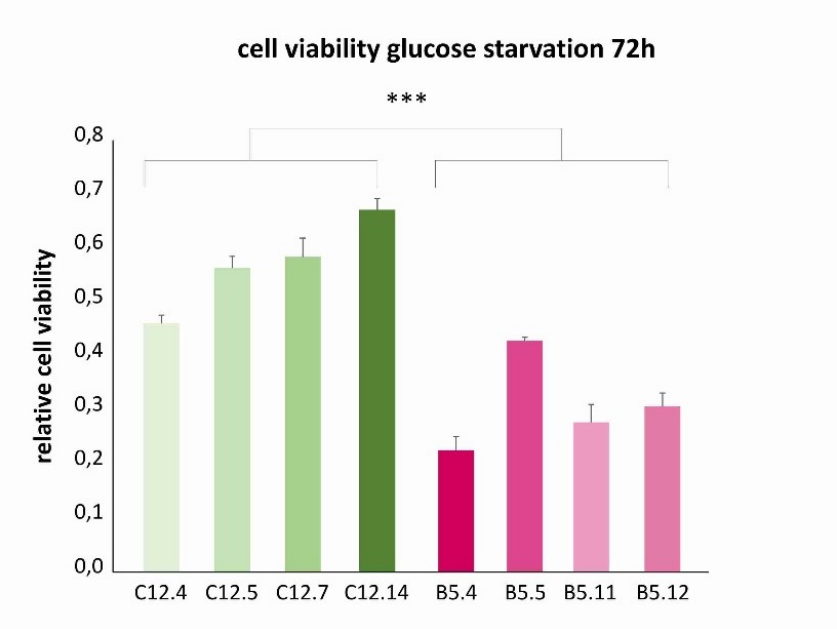

Figure 4

A. Representative SRB assay to evaluate cell viability under glucose starvation at 72 hours**.** Green and pink columns represent GDR and GDS clones, respectively. Columns show mean values ± SD of five biological replicates for each sample. Three independent experiments were performed with similar results (data not shown). Each GDR clone is statistically significant with every GDS clone. ***p<0.001, t test.

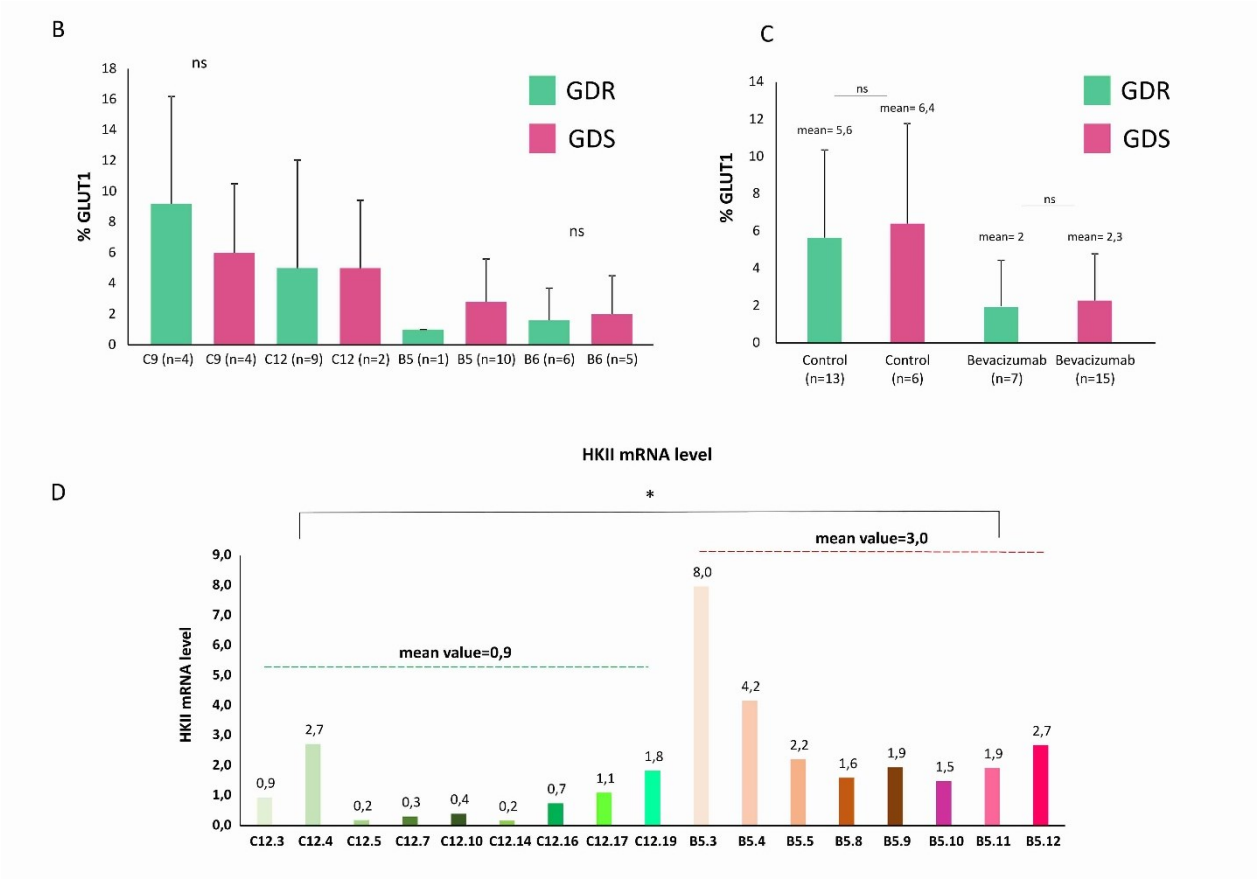

Figure 4

B. Surface expression of GLUT1 by flow cytometry in GDR and GDS clones derived from *ex vivo* cultures of control or Bevacizumab-treated tumors. Statistical analysis was performed only when number of samples was adequate. **C**. Comparison between GDR and GDS clones belonging to CTRL 9,12 and BEVA 5, 6 did not show statistically significant differences. **D**. qRT-PCR analysis showed that GDS clones (pink columns) had higher mean levels of Hexokinase II compared to GDR clones (green columns), albeit with marked variability, * $p<0.05$, t test.

4.5 Pathway differentially expressed in GDS and GDR clones

We performed gene expression profiling of five GDS clones belonging to *ex vivo* culture derived from Bevacizumab-treated tumor (BEVA 5) and five GDR clones belonging to *ex vivo* culture derived from Control tumor (CTRL 12). Results of Gene Set Enrichment Analysis (GSEA) showed that GDS clones had few pathways up-regulated, including apoptosis and O-glycan and several pathways down-regulated, including DNA replication, cell cycle, purine and pyrimidine metabolism among others. The FDR cutoff for significance was set at 0.10. Results are shown in the following table.

Abbreviations in the Table: N. OF GENES = number of genes that contribute to the negative or positive enrichment of the pathway; NES = normalized enrichment score computed by GSEA; FDR = false discovery rate.

Glucose Deprivation Sensitive (GDS) vs Glucose Deprivation Resistant clones (GDR)

PATHWAY DOWN-REGULATED	N. OF GENES	NES	FDR q-value
KEGG_SYSTEMIC_LUPUS_ERYTHEMATOSUS	51	-2,37	0,0000
KEGG_DNA_REPLICATION	25	-2,19	0,0000
KEGG_STEROID_BIOSYNTHESIS	10	-2,05	0,0088
KEGG_RIBOSOME	53	-2,01	0,0122
KEGG_CELL_CYCLE	54	-1,99	0,0125
KEGG_AMINOACYL_TRNA_BIOSYNTHESIS	18	-1,97	0,0145
BIOCARTA_MCM_PATHWAY	14	-1,95	0,0154
KEGG_HOMOLOGOUS_RECOMBINATION	13	-1,90	0,0296
BIOCARTA_COMP_PATHWAY	3	-1,90	0,0265
KEGG_PURINE_METABOLISM	25	-1,91	0,0303
KEGG_SELENOAMINO_ACID_METABOLISM	10	-1,87	0,0312
KEGG_PYRIMIDINE_METABOLISM	41	-1,86	0,0317
KEGG_BASAL_TRANSCRIPTION_FACTORS	17	-1,81	0,0450
KEGG_MISMATCH_REPAIR	13	-1,79	0,0538
BIOCARTA_EIF_PATHWAY	10	-1,77	0,0595
KEGG_TERPENOID_BACKBONE_BIOSYNTHESIS	8	-1,74	0,0697
KEGG_SPLICEOSOME	66	-1,73	0,0689
KEGG_NITROGEN_METABOLISM	7	-1,71	0,0759
KEGG_ONE_CARBON_POOL_BY_FOLATE	11	-1,71	0,0729
KEGG_CALCIUM_SIGNALING_PATHWAY	31	-1,69	0,0852
KEGG_CYSTEINE_AND_METHIONINE_METABOLISM	9	-1,67	0,0917
KEGG_GLYCINE_SERINE_AND_THREONINE_METABOLISM	9	-1,69	0,0914

PATHWAY UP-REGULATED	N. OF GENES	NES	FDR q-value
KEGG_NOD_LIKE_RECEPTOR_SIGNALING_PATHWAY	10	1,87	0,0652
KEGG_O_GLYCAN_BIOSYNTHESIS	8	1,85	0,0495
KEGG_APOPTOSIS	23	1,83	0,0428
BIOCARTA_HIF_PATHWAY	5	1,80	0,0614
BIOCARTA_DEATH_PATHWAY	6	1,79	0,0545

4.6 Differentially regulated transcription factor targets in GDS and GDR clones

In this panel the gene sets, containing targets of transcription factors, significantly enriched in GDS clones compared to GDR clones were reported (FDR<0.05). Bioinformatics analysis showed that in GDS clones the targets of E2F1 are significantly downregulated. Abbreviations in the Table: NES = normalized enrichment score computed by GSEA; FDR = false discovery rate.

Glucose Deprivation Sensitive (GDS) vs Glucose Deprivation Resistant clones (GDR)

TF TARGETS SIGNIFICANTLY DOWN-REGULATED	NES	FDR q-value
KRCTCNNNNMANAGC_UNKNOWN	-2,48	0,0000
TTTNNANAGCYR_UNKNOWN	-2,08	0,0014
V$E2F1_Q6_01	-1,98	0,0045
V$E2F1DP1RB_01	-1,96	0,0050
V$E2F_Q4_01	-1,92	0,0071
V$E2F_Q6_01	-1,91	0,0060
V$E2F1_Q4_01	-1,88	0,0068
V$E2F1_Q3	-1,88	0,0065
V$E2F_Q3	-1,88	0,0058
V$E2F_Q3_01	-1,87	0,0061
V$E2F_03	-1,85	0,0070
ACAWNRNSRCGG_UNKNOWN	-1,80	0,0116
V$E2F_Q4	-1,77	0,0139
V$E2F_Q6	-1,74	0,0189
SGCGSSAAA_V$E2F1DP2_01	-1,73	0,0193
V$CREB_Q3	-1,70	0,0234
V$E2F_01	-1,70	0,0224
V$YY1_02	-1,68	0,0253
V$E2F1_Q6	-1,68	0,0251
RRCCGTTA_UNKNOWN	-1,66	0,0289
GGCNKCCATNK_UNKNOWN	-1,65	0,0302
V$GCM_Q2	-1,65	0,0304
V$E2F4DP1_01	-1,63	0,0328
V$TEF1_Q6	-1,63	0,0324
V$YY1_Q6	-1,63	0,0319
V$E2F1_Q4	-1,61	0,0349
V$NFY_Q6	-1,61	0,0336
GATGKMRGCG_UNKNOWN	-1,60	0,0362
V$E2F_02	-1,60	0,0360
V$E2F1DP1_01	-1,59	0,0385
V$E2F4DP2_01	-1,58	0,0393
V$E2F1DP2_01	-1,58	0,0386
AACYNNNNTTCCS_UNKNOWN	-1,57	0,0416
CCAATNNSNNNGCG_UNKNOWN	-1,57	0,0405
V$AML1_Q6	-1,57	0,0401
V$NFY_Q6_01	-1,56	0,0422
KTGGYRSGAA_UNKNOWN	-1,56	0,0434
V$AML1_01	-1,55	0,0437
V$NFMUE1_Q6	-1,55	0,0446
YYCATTCAWW_UNKNOWN	-1,55	0,0439
GCGNNANTTCC_UNKNOWN	-1,53	0,0483
RYCACNNRNNRNCAG_UNKNOWN	-1,53	0,0482
TF TARGETS SIGNIFICANTLY UP-REGULATED	**NES**	**FDR q-value**
V$ALX4_01	1,84	0,0254
V$NFAT_Q4_01	1,84	0,0127
V$AP1_01	1,83	0,0092
TAAYNRNNTCC_UNKNOWN	1,74	0,0197
V$BACH1_01	1,73	0,0181
V$SRF_C	1,73	0,0162
V$SRF_01	1,68	0,0243
V$HNF6_Q6	1,67	0,0257
V$E2A_Q2	1,65	0,0316
V$AP4_Q5	1,61	0,0461

4.7 Metabolomic analysis of GDR and GDS clones

In parallel, we performed targeted metabolomic analysis of these five GDR and five GDS clones, in collaboration with Dr. Roberta Pastorelli and Dr. Laura Brunelli from the Department of Environmental Health Sciences, IRCCS-Istituto di Ricerche Farmacologiche Mario Negri, Milano. Metabolites were extracted with MeOH/H_2O (85:15) and samples were analyzed using HPLC-QTOF (high pressure liquid chromatography-QTOF) both in positive and negative ionization mode. Negative ionization highlighted mainly polar molecules and amino acids. Positive ionization highlighted mainly amino acids, acyl carnitine and lipids Lipids were not considered in untargeted data elaboration because there were not lipid standards. Differences among samples were investigated using multivariate (PCA/OPLS-DA) or univariate (Wilcoxon-Mann-Whitney, Tukey-Kramer $p<0.05$) statistical analysis.
Preliminary results showed 16 metabolites differentially expressed. GDS samples expressed more Capric acid, Taurine, Spermidine, Glutathione, L-Arginine, Creatine and less 3-Dehydroxycarnitine, L-Acetylcarnitine, Spermine, N-Methylputrescine, Glutamine, Cytidine, Isobutyryl-L-carnitine, 3-Hydroxyanthranilic acid, Isovalerycarnitine and 2-Maleylacetate, compared to GDR clones. Results are shown in the following table.

Metabolites	Fold change
Capric acid	2.23
Taurine	1.87
Spermidine	1.34
Glutathione	1.21
L-Arginine	1.19
Creatine	1.13
3-Dehydroxycarnitine	-1.11
L-Acetylcarnitine	-1.12
Spermine	-1.16
N-Methylputrescine	-1.44
Glutamine	-1.56
Cytidine	-2.47
Isobutyryl-L-carnitine	-3.78
3-Hydroxyanthranilic acid	-4.43
Isovalerylcarnitine	-6.63
2-Maleylacetate	-7.41

4.8 GDS clones express more PKA, CREB, GLS1 and LC3 compared to GDR clones

In a recent work, published by R. Palorini et al., it was demonstrated that cyclic adenosine monophosphate-Protein Kinase A (cAMP-PKA) axis activation is fundamental for cancer cell resistance to glucose starvation and *anoikis*. PKA, through incompletely understood mechanisms, controls several cellular processes like cell growth, cell differentiation and cell metabolism. Upon binding of cAMP to the regulatory subunits, the catalytic subunits of PKA phosphorylate and modulate the activity of a variety of cytosolic and nuclear substrates, including the transcription factor cAMP response element-binding protein (CREB), which modulates glutaminase 1 (GLS1) expression, among other targets. Since BEVA clones were established from an ex vivo culture of a tumor which underwent metabolic stress including glucose starvation, as shown by our previous studies [29], we considered interesting to investigate expression of PKA in clones.

We analyzed PKA and CREB expression by Western blot in collaboration with F. Chiaradonna and H. De Vitto from University of Milano-Bicocca. Intriguingly, preliminary results showed a trend towards increased PKA expression in GDS clones compared to GDR clones (Figure 6). Furthermore, we observed higher CREB phosphorylation, glutamine utilization and autophagy, in according with their published data. Indeed, *Palorini et al.* demonstrated that such a PKA-dependent survival is mediated by parallel activation of autophagy and glutamine utilization that in concert concur to attenuate endoplasmic reticulum (ER) stress and to sustain cell anabolism.

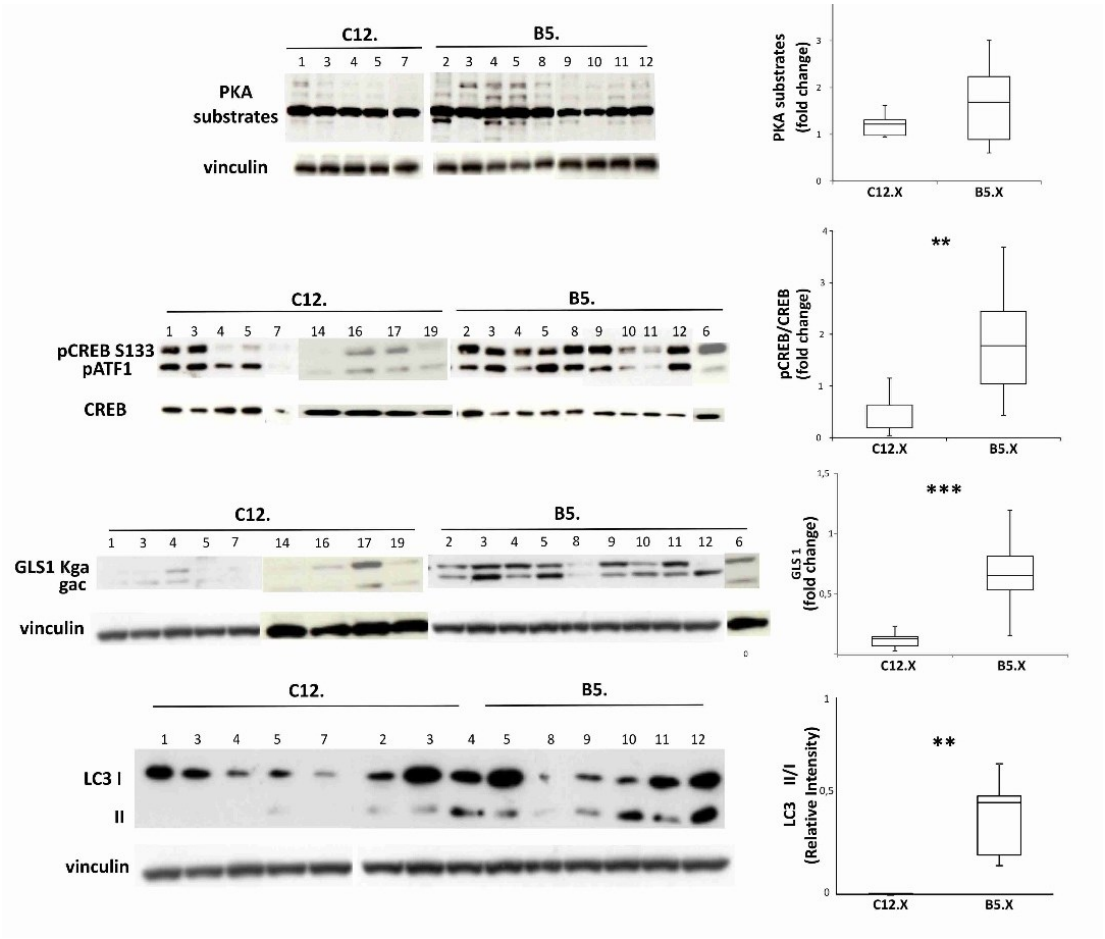

Figure 5

Western blot analysis of GDS clones derived from BEVA 5 culture and GDR clones derived from CTRL 12 culture. GDS clones show higher PKA activity and higher levels of phosphorylation of the transcription factor cAMP response element-binding protein (CREB). They also disclose higher protein levels of glutaminase 1 (GLS1), an enzyme that converts glutamine into glutamate and LC3, a marker of autophagy. ** $p<0.01$, *** $p<0.001$, t test.

4.9 GDR and GDS clones show different kinetics of tumor growth

We finally investigated the tumorigenic behaviour of GDR and GDS clones *in vivo*. To this end, $4x10^5$ cells from five GDR or from five GDS clones were injected subcutaneously in both flanks of SCID mice. In all cases but three, each clone was injected in a mouse, whereas in three cases each clones was injected in two mice. Results showed that GDS derived tumors were invariably smaller compared to GDR derived ones. This finding indirectly confirmed results of transcriptome analysis, which suggested reduced proliferative activity in GDS cells.

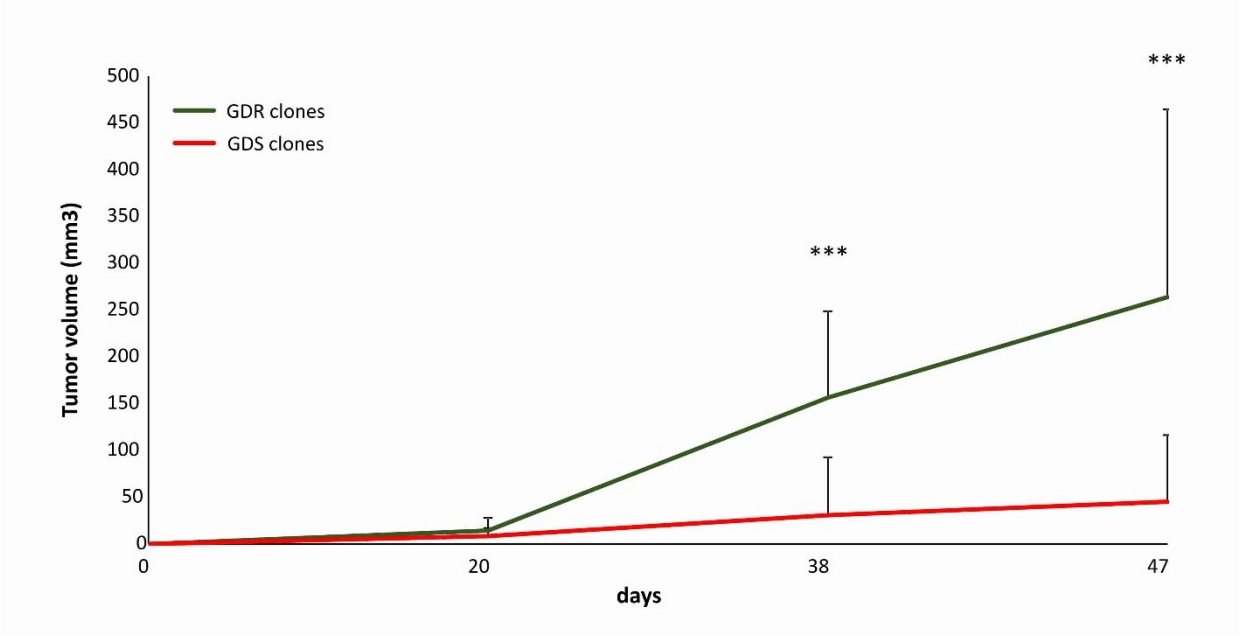

Figure 6

Kinetics of tumor development following subcutaneous injection of GDR (green) and GDS (red) clones. 8 SCID mice (6 wk old, Charles River, Wilmington, MA, USA) for group were subcutaneously injected with $4x10^5$ cells /flank in a 1:1 ratio with Matrigel.

4.10 Western blot analysis of silencing PDHK1 through lentiviral vectors

Stimulated by the finding that tumor cells with high glycolytic activity, as was the case for BEVA cultures (see Figure 1), have accelerated tumor growth compared with less glycolytic tumor cultures, in the second part of my Ph.D work I further investigated the possible connection between the glycolytic phenotype of cancer cells and their tumorigenic potential. To this end, we focused on pyruvate dehydrogenase kinase 1 (PDHK1), an enzyme that sits at key bifurcation point between glycolysis and OXPHOS. Pyruvate dehydrogenase kinase (PDK) is a mitochondrial enzyme that is activated in a variety of cancers and when active it inhibits pyruvate dehydrogenase, a complex of enzymes that converts cytosolic pyruvate to mitochondrial acetyl-CoA, the substrate for the Krebs' cycle. Inhibition of PDK with either small interfering RNAs or the drug dichloroacetate (DCA) shifts metabolism of cancer cells from glycolysis to OXPHOS.

We modulated glycolysis by silencing PDHK1 with shRNA-encoding lentiviral vectors, to stably modulate PDHK1 levels in two highly glycolytic ovarian cancer cell lines (OC316 and OVCAR3). We initially tested four lentiviral vectors to choose the better shRNA construct for subsequent studies. We found strongly reduced levels of target gene expression by q-PCR at different time points after viral transduction (not shown). We analysed PDHK1 protein levels by Western blotting and results demonstrated that both for OC316 and OVCAR3 cell lines all the constructs were efficient (Figure 7). Two vectors, however, (sh6261 for OC316 and sh6260 for OVCAR3) were very efficient in reducing PDHK1 levels, but unfortunately demonstrated high cytotoxic effects and we had to abandon them. So, we continued to performed functional and biological analysis of PDHK1 silencing with the vector sh11007 for the OC316 and the vector sh6263 for the OVCAR3 cell line, because they demonstrated a great reversion of glycolytic phenotype if compared to the others vectors.

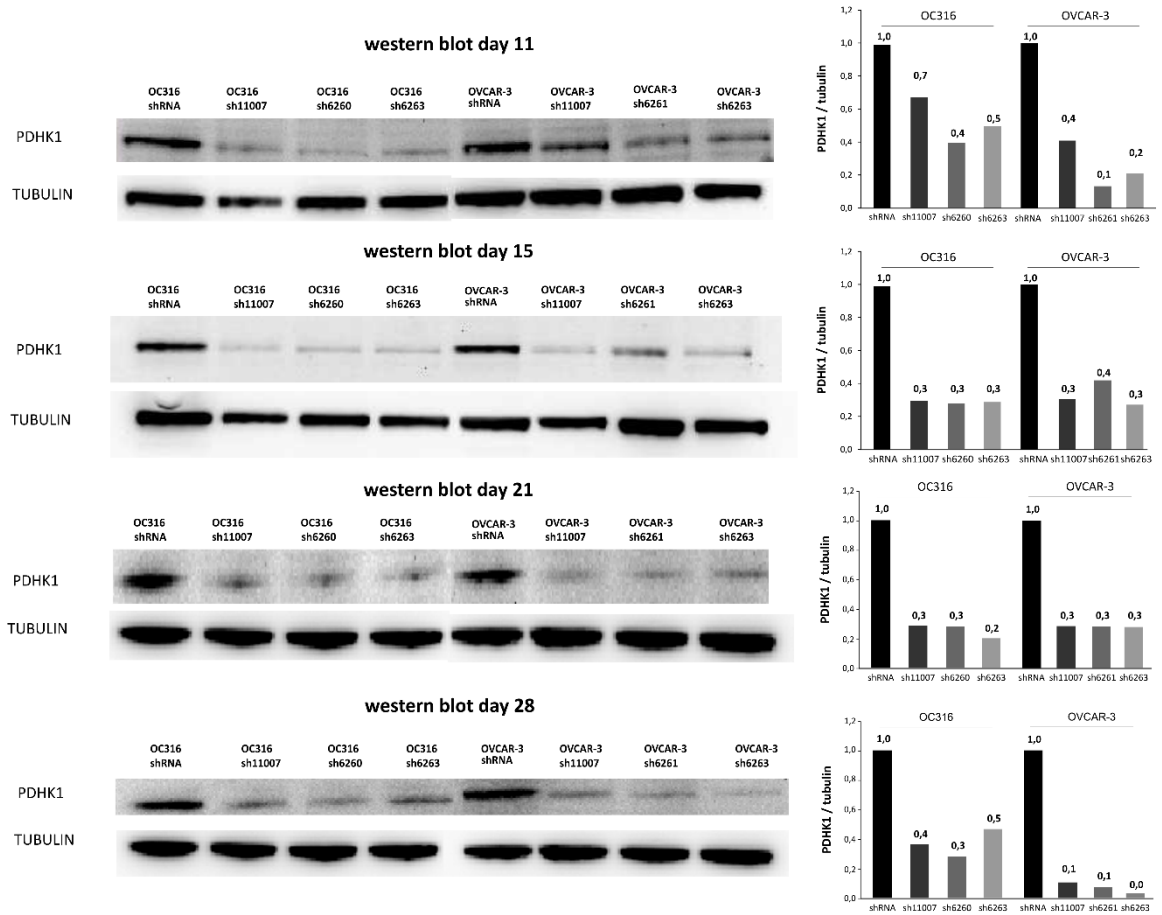

Figure 7

Western blot analysis shows reduction of PDHK1 protein level in cancer cells following delivery of PDHK1-specific shRNAs. Tubulin was used as loading control (left). Quantification of the silencing effect was obtained by normalization of PDHK1 protein level in shPDHK1 cells versus control (right).

4.11 *In vitro* effects of silencing PDHK1 on cell viability

We analyzed effects of silencing PDHK1 on cell proliferation and results, obtained with different assays, showed that PDHK1-deficient cells had decreased cell proliferation compared to control cells.

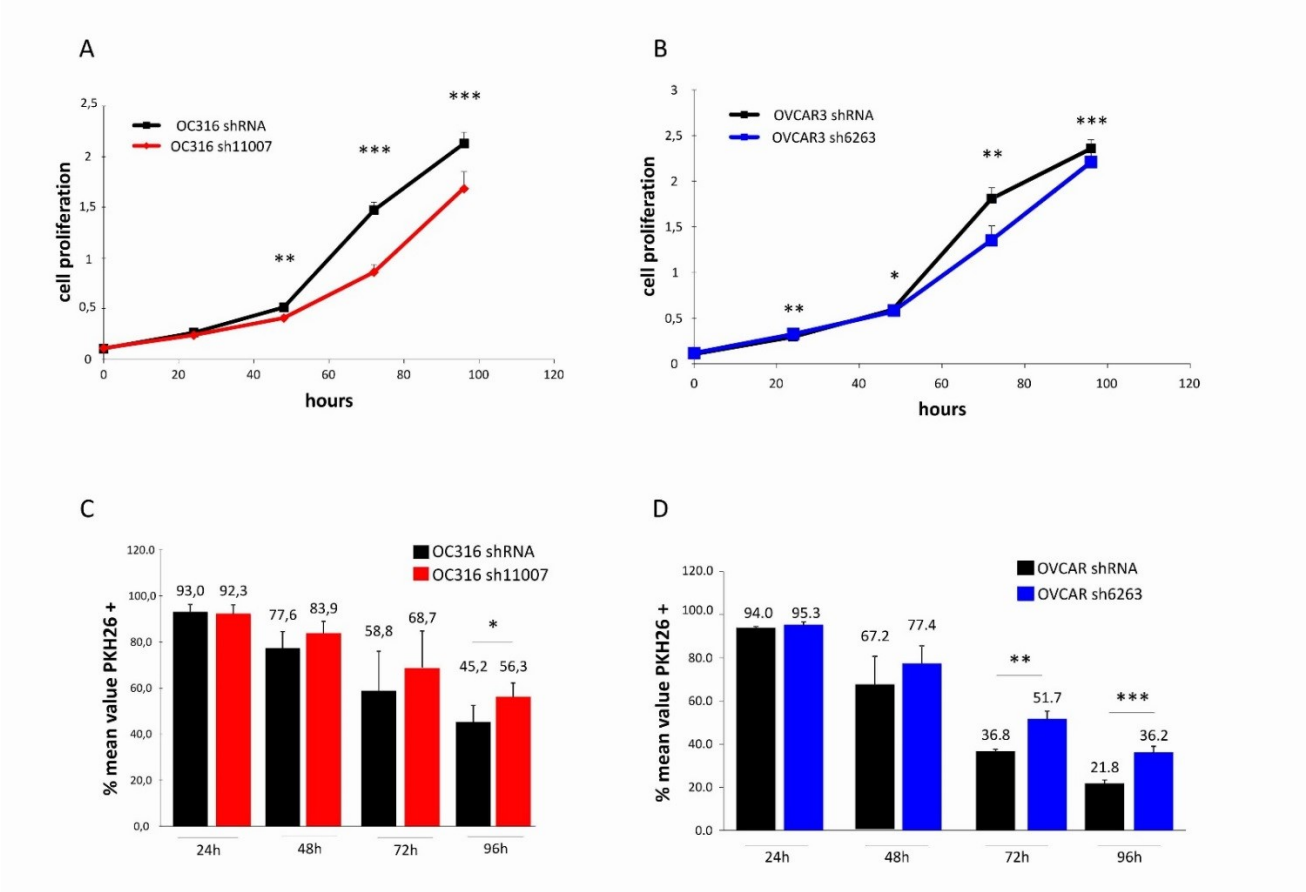

Figure 8

A, B. Results of SRB assays to evaluate cell proliferation at different time points. Columns report mean values ± SD of five different replicates. Representative images of three independent experiments are shown. **p<0.01, ***p<0.001, t test. **C, D**. Measurement of cell division by PKH-26 staining and flow cytometry analysis at different time points. Columns report mean values ± SD of four biological replicates. **p<0.01, ***p<0.001, t test. Both analysis show significant reduction of proliferation rate in OC316 and OVCAR3 shPDHK1 cell lines compared to shRNA.

4.12 The effects of silencing PDHK1 on cell metabolism

We investigated the effects of silencing PDHK1 on cell metabolism and bio energetic analysis by using Seahorse technique showed a significant increase in oxygen consumption rate (OCR) and a decrease in extracellular acidification rate (ECAR) in shPDHK1 cells compared to shRNA cells.

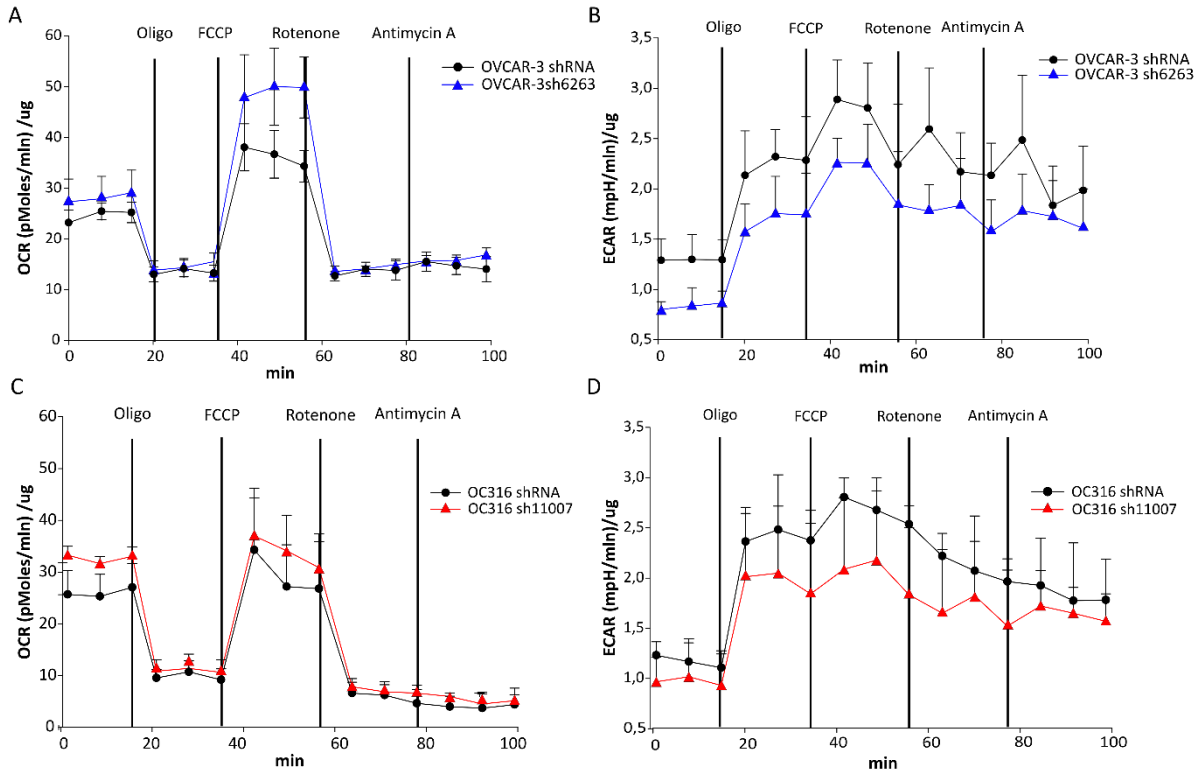

Figure 9

A, B, C, D. Representative bioenergetic analysis shows that shPDHK1 cells become less glycolytic compared to control (shRNA). Specifically, shPDHK1 cells have a significant increase in oxygen consumption rate (OCR) and a decrease in extracellular acidification rate (ECAR). Subsequent additions of the ATP synthase inhibitor oligomycin, of the uncoupler FCCP, of the ETC complex I inhibitor rotenone, and of the respiratory complex III inhibitor antimycin A were carried out as per protocol. Data are mean ± SD values of five replicates normalized to protein content. Analysis was repeated in three independent experiment at different days with similar results.

Then, we investigated cell viability on glucose starvation at 48 hours by analysis of Annexin V/PI staining and the result suggest that PDHK1 silencing is followed by reduced cell death under glucose deprivation.

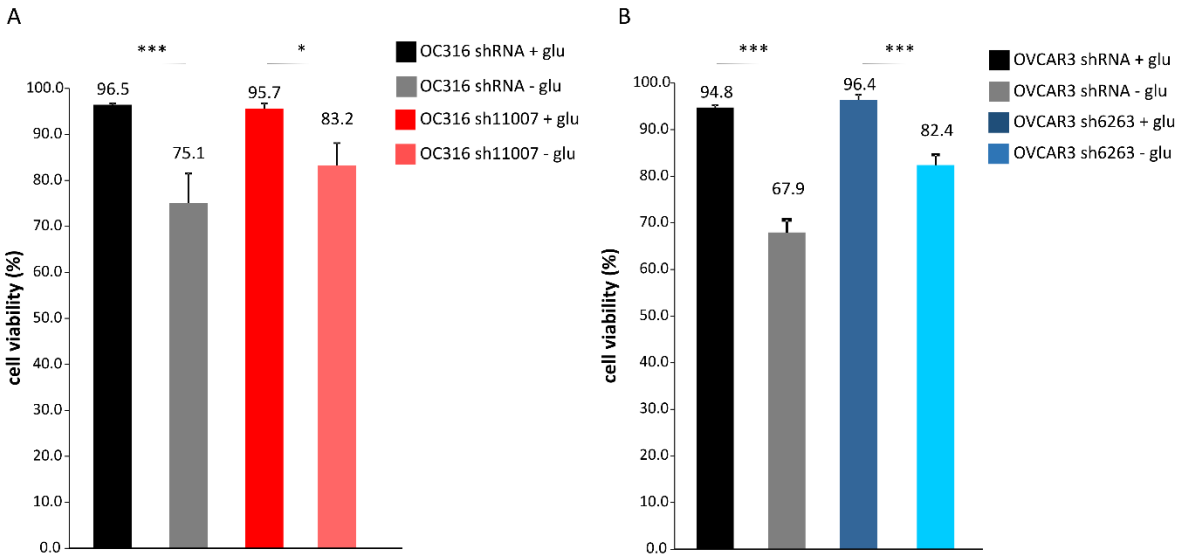

Figure 10

A, B. Cell viability under glucose starvation measured at 48 hours by Annexin V/PI staining. shPDHK1 cells show increased cell viability during glucose starvation compared to control (shRNA) cells. Columns report mean values ± SD for three replicates. **p<0.01, ***p<0.001, t test.

Then, we confirm that shPDHK1 cells are less sensitive to glucose deprivation (panel A), glutamine deprivation (panel B) and both (panel C).

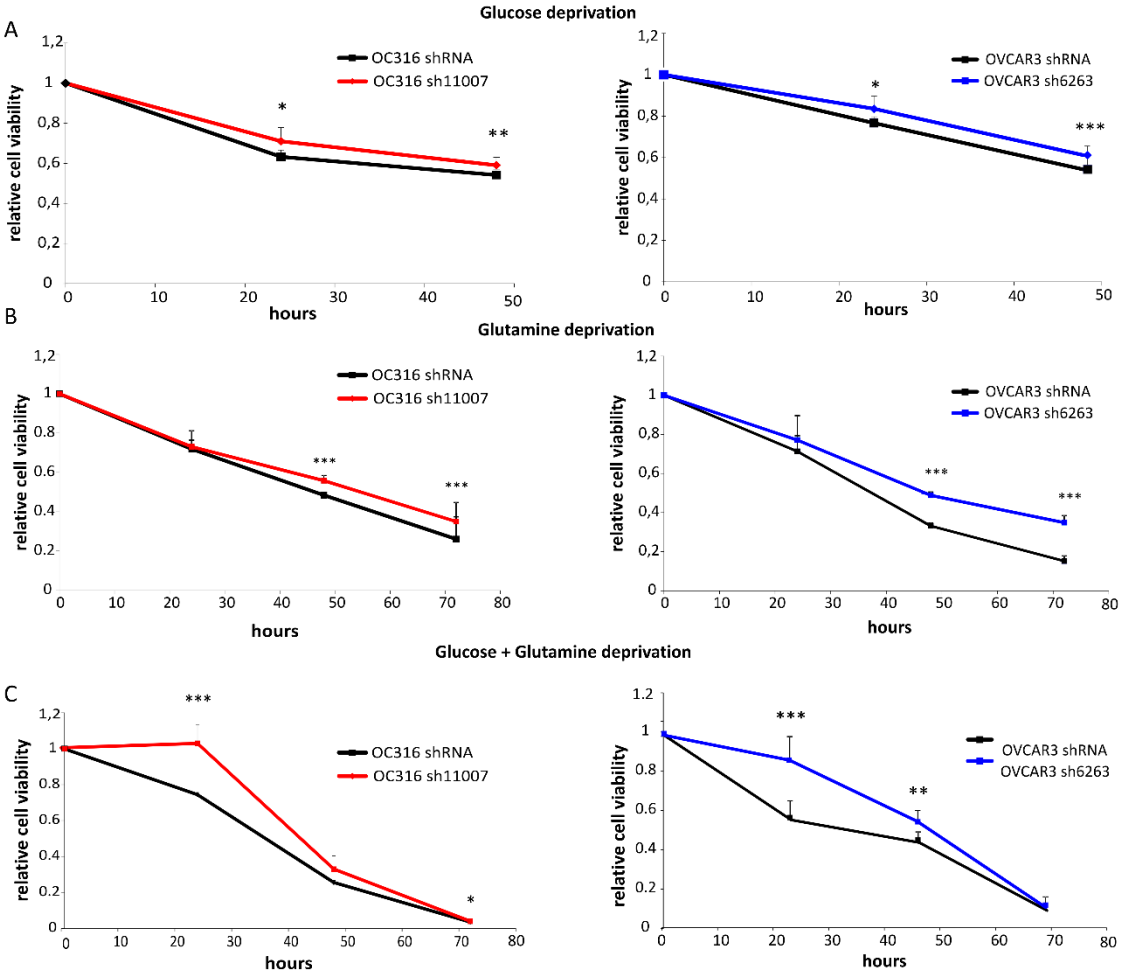

Figure 11

Sulforhodamine B (SRB) colorimetric assay was used to analyse cell viability during glucose starvation (Panel A), glutamine starvation (Panel B) or both (Panel C). Representative images of three independent experiments are shown (five replicates for sample). *p < 0.05, **p<0.01, t test. OC316 and OVCAR3 shPDHK1 cells show a slight but significant reduction of sensibility to metabolic stress compared to control (shRNA) cells.

4.13 *In vivo* effects of silencing PDHK1 on tumor growth

Next, we performed an in vivo experiment to investigate effects of PDHK1 modulation on tumour growth and metabolism. shPDHK1 tumor cells or shRNA cells from OVCAR and OC316 cell lines, were injected subcutaneously in SCID mice (n= 4 mice/group). In both ovarian cancer cell lines, shPDK1 deficient cells formed smaller tumor volumes compared to shRNA cells (Figure 12 A-B). At tumor harvest, we found by qPCR that PDHK1 mRNA expression levels were still reduced in shPDK1 compared to control tumors (Figure 12C). IHC analysis showed that in both models shRNA tumors had more necrotic areas compared to shPDHK1 tumors (Figure 12D).

Finally, tumours obtained from PDHK1-deficient cells have less p-HH3, a marker of cell proliferation, compared to controls (Figure 12E).

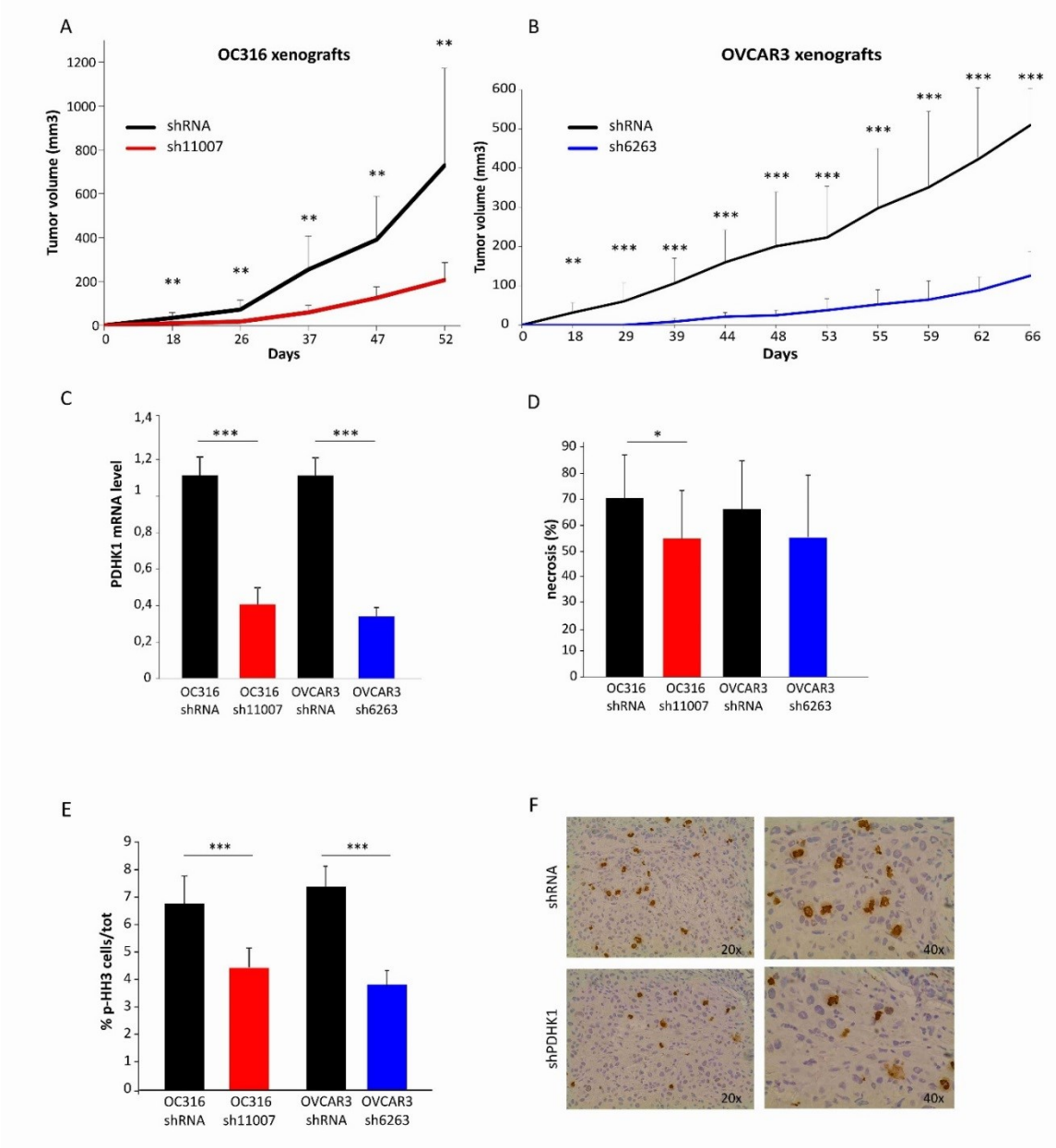

Figure 12

A. Kinetics of tumor development following subcutaneous injection of OC316 shRNA (black) and OC316 shPDHK1 (red) tumor cells in SCID mice. Four SCID mice (6 wk old, Charles River, Wilmington, MA, USA) per group were subcutaneously injected with 4x105 cells /flank in a 1:1 ratio with Matrigel. **B**. The panel shows similar results obtained in the OVCAR3 model. Curves indicate mean tumor volume values ± SD for eight samples/group. **p<0.01, ***p<0.001. **C**. Q-RT-PCR analysis of PDHK1 transcripts in tumors after the sacrifice to confirm the silencing. Columns show mean ± SD values of duplicate determinations of eight samples per group. ***p<0.001. **D**. Columns indicate quantitative analysis of necrotic areas in n = 5-10 fields per tumor; n= 8 different tumors per group. Histologic analysis shows a trend towards increased necrotic areas in shRNA tumors compared to shPDHK1 tumors. **E.** Evaluation of proliferation in tumors by phospho-Histone-H3 (p-HH3)

staining, a nuclear proliferation marker specific for cells undergoing mitosis. The columns indicate mean ± SD values; 8 samples per group were analyzed. ***P < 0.001, compared with the control group. **F**. Representative IHC images of OC316 shRNA and sh11007 tumors (original magnification: ×20 and x40).

4.14 The effects of silencing PDHK1 on angiogenesis

Finally, we studied the relationship between metabolism and angiogenesis. First, we calculated micro vessel density (MVD) by immunohistochemistry analysis of CD31+ cells and results showed that PDHK1 silenced tumors had not only significantly reduced MVD, compared to controls, but also marked variations in vessel diameter and shape.

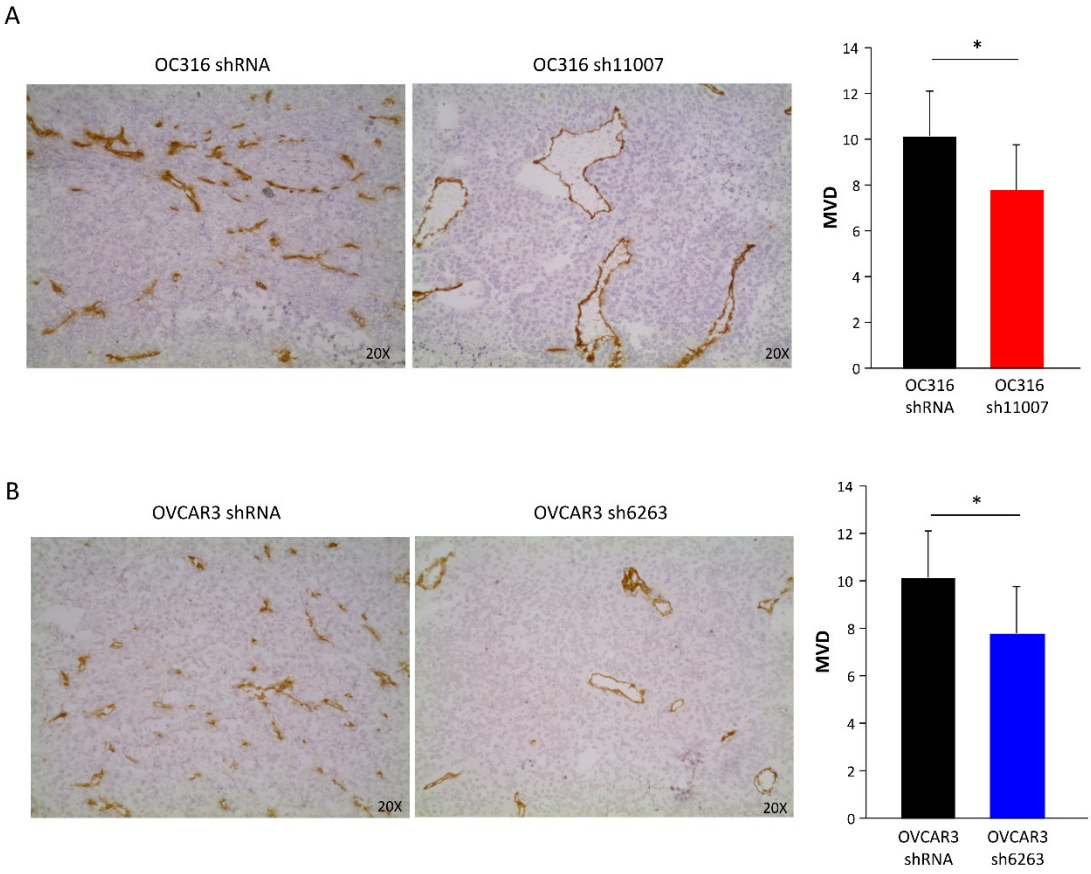

Figure 13

A. Representative images of CD31+ vascular cells in OC316 shRNA and in OC316 sh11007 tumors. Right; Columns show mean ± SD values of seven tumors for each group. *p<0.05 (right). **B**. Similar results in the OVCAR3 model.

4.15 Transcriptome analysis of shPDHK1 and shRNA in OVCAR3 model

Furthermore, we performed transcriptome analysis of five OVCAR3 shRNA tumors and five shPDHK1 tumors sacrificed at equivalent tumor volumes. Bioinformatics analysis (GSEA) showed that PDHK1 deficient tumors had several up-regulated pathways, including cell cycle, N-Glycan biosynthesis, Fructose and Mannose metabolism, Pentose phosphate pathway and Valine, Leucine, Isoleucine degradation.

Abbreviations in the Table: N. OF GENES = number of genes that contribute to the negative or positive enrichment of the pathway; NES = normalized enrichment score computed by GSEA; FDR = false discovery rate.

OVCAR3 shPDHK1 versus OVCAR3 shRNA tumors

PATHWAY SIGNIFICANTLY DOWN-REGULATED	N. OF GENES	NES	FDR q-value
BIOCARTA_ALK_PATHWAY	5	-1,88	0,0834374
PATHWAY SIGNIFICANTLY UP-REGULATED	**N. OF GENES**	**NES**	**FDR q-value**
BIOCARTA_CELLCYCLE_PATHWAY	8	2,00	0,0607
KEGG_N_GLYCAN_BIOSYNTHESIS	19	1,98	0,0431
KEGG_FRUCTOSE_AND_MANNOSE_METABOLISM	8	1,89	0,0791
KEGG_PENTOSE_PHOSPHATE_PATHWAY	7	1,83	0,1067
BIOCARTA_G1_PATHWAY	7	1,83	0,0916
KEGG_VALINE_LEUCINE_AND_ISOLEUCINE_DEGRADATION	10	1,81	0,0898

4.16 Differentially regulated transcription factor targets in OVCAR3 shPDHK1 and shRNA

In this panel the gene sets, containing targets of transcription factors, significantly downregulated in OVCAR3 shPDHK1 tumors compared to shRNA tumors were reported (FDR<0.10). No significantly upregulated pathways were found with FDR cutoff set at 0.10. Abbreviations in the Table: NES = normalized enrichment score computed by GSEA; FDR = false discovery rate.

OVCAR3 shPDHK1 versus OVCAR3 shRNA tumors

TF TARGETS SIGNIFICANTLY DOWN-REGULATED	NES	FDR q-value
GCGSCMNTTT_UNKNOWN	-1,85	0,0647
V$E2F1_Q4_01	-1,79	0,0725
TTCNRGNNNNTTC_V$HSF_Q6	-1,77	0,0619
V$E2F1DP2_01	-1,75	0,0541
V$E2F_02	-1,75	0,0487
V$E2F4DP2_01	-1,74	0,0417
V$E2F1DP1_01	-1,74	0,0376
V$E2F4DP1_01	-1,70	0,0554
V$E2F1_Q6	-1,69	0,0548
V$E2F_Q3_01	-1,67	0,0678
V$E2F_Q4	-1,66	0,0655
V$E2F_Q6	-1,66	0,0606
V$GR_01	-1,64	0,0688
V$OCT1_04	-1,64	0,0681
V$FOXM1_01	-1,63	0,0741
CCAATNNSNNNGCG_UNKNOWN	-1,62	0,0703
V$NKX25_02	-1,61	0,0771
V$E2F1_Q6_01	-1,60	0,0805
V$IRF1_01	-1,59	0,0907
V$PAX4_04	-1,59	0,0884
V$PBX1_02	-1,57	0,0947
KCCGNSWTTT_UNKNOWN	-1,57	0,0945
RGAANNTTC_V$HSF1_01	-1,56	0,0975
V$OCT1_05	-1,56	0,0942
GGCNRNWCTTYS_UNKNOWN	-1,56	0,0967
V$OCT1_07	-1,55	0,0944
V$PITX2_Q2	-1,55	0,0944
ACAWYAAAG_UNKNOWN	-1,55	0,0912

5. DISCUSSION (1st part)

In the first part of the project, we confirmed that Bevacizumab treatment stably up-modulates the glycolytic phenotype of tumor cells in EOC xenografts and that such metabolic adaptation correlates with increased tumor aggressiveness, as previously reported. In our previous experiments, however, we did not investigate the possible metabolic heterogeneity in tumor-derived cultures and my work started at this point to better characterize the metabolic and molecular changes associated with anti-VEGF therapy in tumors. Our hypothesis was that targeted therapies impacting on tumor angiogenesis could lead to selection of metabolic variants poorly represented in the original tumor, which could bear druggable metabolic vulnerabilities. To investigate this hypothesis, we initially tried to purify by sorting tumor cell subpopulations with increased uptake of the glucose analogue 2-NBDG, but results showed that this phenotype – based on assessment of 2-NBDG expression - was not stable. Therefore, we subsequently investigated whether we could identify clones of tumor cells endowed with different metabolic features by a glucose starvation assay, postulating that highly glycolytic tumor cells could be more glucose addicted compared with poorly glycolytic tumor cells. In this assay, glucose-addicted clones were termed GDS and those less glucose addicted were termed GDR. This assumption was initially tested and substantially confirmed in clones derived from the OC316 and IGROV-1 tumor cell lines, well known for their highly or poorly glycolytic profile. However, results seemed at odds with the hypothesis when clones derived from ex vivo cultures of IGROV-1 tumors were examined. Overall, we obtained and analyzed n=109 clones from Control tumors and n=87 clones from Bevacizumab-treated tumors. In control tumors-derived clones, proportions of GDR and GDS clones were 53% and 47%, respectively. Notably, these proportions were close to those measured in the parental IGROV-1 cells line (55% and 45%, respectively). In contrast, clones derived from bevacizumab-treated tumors contained 63% and 37% of GDR and GDS type, respectively. This result was unexpected, because we knew that bevacizumab selects for the highly glycolytic phenotype, as also indicated by results of Seahorse analysis and lactate production measurements in ex vivo tumor cell cultures. Therefore, we expected to detect enrichment of glucose addicted GDS clones in tumor cultures from bevacizumab-treated tumors. The finding that there might indeed be enrichment of GDR clones could indicate that tumor cultures contain probably a mix of cells with different glycolytic properties, including both GDS and GDR types, but then at the clonal level we preferentially expanded GDR cells, may be due to a proliferative

advantage in vitro. In this regard, results of transcriptome analysis fit this explanation, as they highlighted impaired DNA synthesis and cell cycle-associated transcripts in GDS compared with GDR clones.

Alternatively, it could be that bevacizumab treatment by lowering glucose and ATP levels in tumors, as shown by metabolic imaging in our previous study (Nardo G. et al.), favors selection of cells relatively resistant to glucose starvation, such as GDR clones. Along this line, it is interesting to observe that we found increased PKA activity in clones established from a bevacizumab-treated tumor (albeit classified as GDS clones), a kinase whose expression has been found increased under glucose starvation. Recently, Palorini et al. demonstrated that cyclic adenosine monophosphate-Protein Kinase A (cAMP-PKA) axis activation is fundamental for cancer cell resistance to glucose starvation and anoikis [90]. To further investigate this hypothesis, it will be important to analyze PKA and CREB activation in ex vivo cultures obtained from Control and Bevacizumab groups and also in both GDS and GDR clones both derived from bevacizumab-treated tumors.

If these upcoming experiments will confirm increased PKA activation in ex vivo cultures derived from bevacizumab- treated tumors, we will further study the role of PKA in the metabolic changes associate with anti-VEGF therapy. Importantly, a recent work by Semenza found an interaction between PKA and HIF1α, showing that PKA could increase HIF-1 activity under hypoxic conditions [91]. Indeed, HIF-1α targets were among those up-regulated in GDS clones in our GEP analysis.

Furthermore, GSEA (Gene Set Enrichment Analysis) showed that GDS clones had as a pathway up-regulated apoptosis and cell cycle and DNA replication. These findings were confirmed by an in vivo experiment, which showed that GDS are less tumorigenic compared to GDR clones. Therefore, the functional role of GDS clones in the context of the tumor remains somewhat puzzling, as these clones would seem disadvantaged compared to GDR clones, yet they are relatively conserved in tumors. Future studies are needed to clarify these issues. Among them, since our experiments were so far performed in the early anti-VEGF resistance phase of tumor growth, it will be important to obtain new tumor samples representative of a fully bevacizumab-resistant disease, and perform some of the above described studies in these samples.

DISCUSSION (2nd part)

Concerning the second part of the project, we demonstrated that PDHK1 inactivation was associated with reduced in vitro cell proliferation and in vivo tumor growth. One possible explanation was that silencing of PDHK1 and the consequent increase of OXPHOS could produce higher levels of reactive oxygen species (ROS) in PDHK1 deficient cells (shPDHK1), compared to control cells (shRNA). This hypothetical alteration in ROS homeostasis could lead to cell death. However, we did not find any significant difference in terms of ROS production, measured by mitosoxRed labelling followed by flow cytometry analysis, or IHC staining for 8-oxoguanine in tumors, between shPDHK1 and shRNA tumor cells. Further, analysis on cell death by Annexin V/PI assay, as well as measurements of activated caspase 3 or cleaved PARP protein levels, disclosed similar levels of apoptosis in all samples analyzed. We speculate that upregulation of penthose phosphate pathway (PPP) in shPDHK1-deficient tumor cells, as found by GSEA, could increase ROS scavengers in tumor cells, thus attenuating effects of increased OXPHOS activity on ROS homeostasis. The pentose phosphate pathway indeed generates NADPH, which is required for the regeneration of reduced glutathione (GSH),that is in turn used by glutathione peroxidase (GPX) to eliminate H2O2. Consequently, higher NAPDH levels allow more efficient ROS degradation and this may be the reason why shPDHK1 cells maintain cell viability.

As alternative explanation for the results obtained we should stress that we found significant downregulation of E2F1 in shPDHK1 cells, a transcription factor which plays a crucial role in the control of cell cycle. Indeed, the oncosuppressor Rb binds E2F1, preventing cell cycle progression. Down regulation of E2F1 targets might thus imply suppression of E2F1 by Rb and explain reduced cell cycle progression, as detected in shPDHK1 silenced cells. Future experiments will be performed to analyze expression of pRb/Rb in these cells.

Moreover, we demonstrated that silencing of PDHK1 in OC316 and OVCAR3 cells was associated with a different metabolic profile compared to the shRNA OC316 and OVCAR3 cells. Bio energetic analysis by Seahorse showed a significant increase in OCR and a decrease ECAR in shPDHK1 cells compared to shRNA cells. We also demonstrated that shPDHK1 cells were less sensitive to glucose deprivation, glutamine deprivation or both nutrients together compared to shRNA cells.

In addition, we investigated the correlation between glycolytic activity and angiogenesis and we found that PDHK1 deficient tumors had not only significantly reduced microvessel density, compared to controls, but had also marked variations in vessel diameter and shape. Further analysis will be conducted to investigate vessel perfusion in shPDHK1 and shRNA tumors. Moreover, additional in vitro experiments will be done through ELISA assay to evaluate production of VEGF and other pro-angiogenic factors by these cells.

In conclusion, we demonstrated that PDHK1 inactivation was associated with reduced cell proliferation and altered angiogenesis in experimental tumors, suggesting that metabolic drugs targeting glycolysis might also indirectly affect tumor angiogenesis.

6. REFERENCES

1. Jemal, A., et al., *Cancer statistics, 2008.* CA Cancer J Clin, 2008. **58**(2): p. 71-96.
2. Stratton, M.R., *Exploring the genomes of cancer cells: progress and promise.* Science, 2011. **331**(6024): p. 1553-8.
3. Hanahan, D. and R.A. Weinberg, *Hallmarks of cancer: the next generation.* Cell, 2011. **144**(5): p. 646-74.
4. Bast, R.C., Jr., B. Hennessy, and G.B. Mills, *The biology of ovarian cancer: new opportunities for translation.* Nat Rev Cancer, 2009. **9**(6): p. 415-28.
5. Tjalma, W.A., *Staging classification for cancer of the ovary and the fallopian tube should include in situ carcinoma.* J Gynecol Oncol, 2015. **26**(4): p. 355-6.
6. Kim, A., et al., *Therapeutic strategies in epithelial ovarian cancer.* J Exp Clin Cancer Res, 2012. **31**: p. 14.
7. Conteduca, V., et al., *The emerging role of anti-angiogenic therapy in ovarian cancer (review).* Int J Oncol, 2014. **44**(5): p. 1417-24.
8. Rudlowski, C., et al., *Prognostic significance of vascular endothelial growth factor expression in ovarian cancer patients: a long-term follow-up.* Int J Gynecol Cancer, 2006. **16 Suppl 1**: p. 183-9.
9. Kroep, J.R. and J.W. Nortier, *The role of bevacizumab in advanced epithelial ovarian cancer.* Curr Pharm Des, 2012. **18**(25): p. 3775-83.
10. Risau, W. and I. Flamme, *Vasculogenesis.* Annu Rev Cell Dev Biol, 1995. **11**: p. 73-91.
11. Leung, D.W., et al., *Vascular endothelial growth factor is a secreted angiogenic mitogen.* Science, 1989. **246**(4935): p. 1306-9.
12. Neufeld, G., et al., *Vascular endothelial growth factor and its receptors.* Prog Growth Factor Res, 1994. **5**(1): p. 89-97.
13. Olsson, A.K., et al., *VEGF receptor signalling - in control of vascular function.* Nat Rev Mol Cell Biol, 2006. **7**(5): p. 359-71.
14. Herr, D., et al., *VEGF induces ascites in ovarian cancer patients via increasing peritoneal permeability by downregulation of Claudin 5.* Gynecol Oncol, 2012. **127**(1): p. 210-6.
15. Bekes, I., et al., *Does VEGF facilitate local tumor growth and spread into the abdominal cavity by suppressing endothelial cell adhesion, thus increasing vascular peritoneal permeability followed by ascites production in ovarian cancer?* Mol Cancer, 2016. **15**: p. 13.
16. Masoumi Moghaddam, S., et al., *Significance of vascular endothelial growth factor in growth and peritoneal dissemination of ovarian cancer.* Cancer Metastasis Rev, 2012. **31**(1-2): p. 143-62.
17. Folkman, J., et al., *Isolation of a tumor factor responsible for angiogenesis.* J Exp Med, 1971. **133**(2): p. 275-88.
18. McIntyre, A. and A.L. Harris, *Metabolic and hypoxic adaptation to anti-angiogenic therapy: a target for induced essentiality.* EMBO Mol Med, 2015. **7**(4): p. 368-79.
19. Vasudev, N.S. and A.R. Reynolds, *Anti-angiogenic therapy for cancer: current progress, unresolved questions and future directions.* Angiogenesis, 2014. **17**(3): p. 471-94.
20. Carmeliet, P. and R.K. Jain, *Molecular mechanisms and clinical applications of angiogenesis.* Nature, 2011. **473**(7347): p. 298-307.
21. Crawford, Y., et al., *PDGF-C mediates the angiogenic and tumorigenic properties of fibroblasts associated with tumors refractory to anti-VEGF treatment.* Cancer Cell, 2009. **15**(1): p. 21-34.
22. Gerber, H.P. and N. Ferrara, *Pharmacology and pharmacodynamics of bevacizumab as monotherapy or in combination with cytotoxic therapy in preclinical studies.* Cancer Res, 2005. **65**(3): p. 671-80.

23. Leite de Oliveira, R., A. Hamm, and M. Mazzone, *Growing tumor vessels: more than one way to skin a cat - implications for angiogenesis targeted cancer therapies.* Mol Aspects Med, 2011. **32**(2): p. 71-87.
24. Bergers, G. and D. Hanahan, *Modes of resistance to anti-angiogenic therapy.* Nat Rev Cancer, 2008. **8**(8): p. 592-603.
25. Giuliano, S. and G. Pages, *Mechanisms of resistance to anti-angiogenesis therapies.* Biochimie, 2013. **95**(6): p. 1110-9.
26. Kerbel, R.S., *Issues regarding improving the impact of antiangiogenic drugs for the treatment of breast cancer.* Breast, 2009. **18 Suppl 3**: p. S41-7.
27. Rossi, L., et al., *Bevacizumab in ovarian cancer: A critical review of phase III studies.* Oncotarget, 2016.
28. Escudier, B., et al., *Phase III trial of bevacizumab plus interferon alfa-2a in patients with metastatic renal cell carcinoma (AVOREN): final analysis of overall survival.* J Clin Oncol, 2010. **28**(13): p. 2144-50.
29. Jimenez-Valerio, G., et al., *Resistance to Antiangiogenic Therapies by Metabolic Symbiosis in Renal Cell Carcinoma PDX Models and Patients.* Cell Rep, 2016. **15**(6): p. 1134-43.
30. de Gramont, A., et al., *Bevacizumab plus oxaliplatin-based chemotherapy as adjuvant treatment for colon cancer (AVANT): a phase 3 randomised controlled trial.* Lancet Oncol, 2012. **13**(12): p. 1225-33.
31. Ellis, L.M. and D.J. Hicklin, *Pathways mediating resistance to vascular endothelial growth factor-targeted therapy.* Clin Cancer Res, 2008. **14**(20): p. 6371-5.
32. Clarke, J.M. and H.I. Hurwitz, *Understanding and targeting resistance to anti-angiogenic therapies.* J Gastrointest Oncol, 2013. **4**(3): p. 253-63.
33. Welti, J., et al., *Recent molecular discoveries in angiogenesis and antiangiogenic therapies in cancer.* J Clin Invest, 2013. **123**(8): p. 3190-200.
34. Rigamonti, N., et al., *Role of angiopoietin-2 in adaptive tumor resistance to VEGF signaling blockade.* Cell Rep, 2014. **8**(3): p. 696-706.
35. Jahangiri, A., et al., *Gene expression profile identifies tyrosine kinase c-Met as a targetable mediator of antiangiogenic therapy resistance.* Clin Cancer Res, 2013. **19**(7): p. 1773-83.
36. Bottsford-Miller, J.N., R.L. Coleman, and A.K. Sood, *Resistance and escape from antiangiogenesis therapy: clinical implications and future strategies.* J Clin Oncol, 2012. **30**(32): p. 4026-34.
37. Casanovas, O., et al., *Drug resistance by evasion of antiangiogenic targeting of VEGF signaling in late-stage pancreatic islet tumors.* Cancer Cell, 2005. **8**(4): p. 299-309.
38. De Bock, K., M. Mazzone, and P. Carmeliet, *Antiangiogenic therapy, hypoxia, and metastasis: risky liaisons, or not?* Nat Rev Clin Oncol, 2011. **8**(7): p. 393-404.
39. Harris, A.L., *Hypoxia--a key regulatory factor in tumour growth.* Nat Rev Cancer, 2002. **2**(1): p. 38-47.
40. Schulze, A. and A.L. Harris, *How cancer metabolism is tuned for proliferation and vulnerable to disruption.* Nature, 2012. **491**(7424): p. 364-73.
41. Kumar, K., et al., *Dichloroacetate reverses the hypoxic adaptation to bevacizumab and enhances its antitumor effects in mouse xenografts.* J Mol Med (Berl), 2013. **91**(6): p. 749-58.
42. Curtarello, M., et al., *VEGF-targeted therapy stably modulates the glycolytic phenotype of tumor cells.* Cancer Res, 2015. **75**(1): p. 120-33.
43. Ullah, M.S., A.J. Davies, and A.P. Halestrap, *The plasma membrane lactate transporter MCT4, but not MCT1, is up-regulated by hypoxia through a HIF-1alpha-dependent mechanism.* J Biol Chem, 2006. **281**(14): p. 9030-7.
44. Sonveaux, P., et al., *Targeting lactate-fueled respiration selectively kills hypoxic tumor cells in mice.* J Clin Invest, 2008. **118**(12): p. 3930-42.
45. Allen, E., et al., *Metabolic Symbiosis Enables Adaptive Resistance to Anti-angiogenic Therapy that Is Dependent on mTOR Signaling.* Cell Rep, 2016. **15**(6): p. 1144-60.

46. Pisarsky, L., et al., *Targeting Metabolic Symbiosis to Overcome Resistance to Anti-angiogenic Therapy.* Cell Rep, 2016. **15**(6): p. 1161-74.
47. Cantor, J.R. and D.M. Sabatini, *Cancer cell metabolism: one hallmark, many faces.* Cancer Discov, 2012. **2**(10): p. 881-98.
48. Warburg, O., *On the origin of cancer cells.* Science, 1956. **123**(3191): p. 309-14.
49. Moreno-Sanchez, R., et al., *Energy metabolism in tumor cells.* FEBS J, 2007. **274**(6): p. 1393-418.
50. Zulato, E., et al., *Metabolic effects of anti-angiogenic therapy in tumors.* Biochimie, 2012. **94**(4): p. 925-31.
51. Vander Heiden, M.G., L.C. Cantley, and C.B. Thompson, *Understanding the Warburg effect: the metabolic requirements of cell proliferation.* Science, 2009. **324**(5930): p. 1029-33.
52. Pavlova, N.N. and C.B. Thompson, *The Emerging Hallmarks of Cancer Metabolism.* Cell Metab, 2016. **23**(1): p. 27-47.
53. Yang, L., et al., *Metabolic shifts toward glutamine regulate tumor growth, invasion and bioenergetics in ovarian cancer.* Mol Syst Biol, 2014. **10**: p. 728.
54. DeBerardinis, R.J. and N.S. Chandel, *Fundamentals of cancer metabolism.* Sci Adv, 2016. **2**(5): p. e1600200.
55. Shim, H., et al., *c-Myc transactivation of LDH-A: implications for tumor metabolism and growth.* Proc Natl Acad Sci U S A, 1997. **94**(13): p. 6658-63.
56. Wahlstrom, T. and M.A. Henriksson, *Impact of MYC in regulation of tumor cell metabolism.* Biochim Biophys Acta, 2015. **1849**(5): p. 563-9.
57. Vousden, K.H. and K.M. Ryan, *p53 and metabolism.* Nat Rev Cancer, 2009. **9**(10): p. 691-700.
58. Madan, E., et al., *Regulation of glucose metabolism by p53: emerging new roles for the tumor suppressor.* Oncotarget, 2011. **2**(12): p. 948-57.
59. Matoba, S., et al., *p53 regulates mitochondrial respiration.* Science, 2006. **312**(5780): p. 1650-3.
60. Mathupala, S.P., A. Rempel, and P.L. Pedersen, *Glucose catabolism in cancer cells: identification and characterization of a marked activation response of the type II hexokinase gene to hypoxic conditions.* J Biol Chem, 2001. **276**(46): p. 43407-12.
61. Wigfield, S.M., et al., *PDK-1 regulates lactate production in hypoxia and is associated with poor prognosis in head and neck squamous cancer.* Br J Cancer, 2008. **98**(12): p. 1975-84.
62. Ying, H., et al., *Oncogenic Kras maintains pancreatic tumors through regulation of anabolic glucose metabolism.* Cell, 2012. **149**(3): p. 656-70.
63. Nagarajah, J., et al., *Correlation of BRAFV600E Mutation and Glucose Metabolism in Thyroid Cancer Patients: An (1)(8)F-FDG PET Study.* J Nucl Med, 2015. **56**(5): p. 662-7.
64. Granchi, C. and F. Minutolo, *Anticancer agents that counteract tumor glycolysis.* ChemMedChem, 2012. **7**(8): p. 1318-50.
65. Walenta, S., T. Schroeder, and W. Mueller-Klieser, *Lactate in solid malignant tumors: potential basis of a metabolic classification in clinical oncology.* Curr Med Chem, 2004. **11**(16): p. 2195-204.
66. Brizel, D.M., et al., *Elevated tumor lactate concentrations predict for an increased risk of metastases in head-and-neck cancer.* Int J Radiat Oncol Biol Phys, 2001. **51**(2): p. 349-53.
67. Beckert, S., et al., *Lactate stimulates endothelial cell migration.* Wound Repair Regen, 2006. **14**(3): p. 321-4.
68. Vegran, F., et al., *Lactate influx through the endothelial cell monocarboxylate transporter MCT1 supports an NF-kappaB/IL-8 pathway that drives tumor angiogenesis.* Cancer Res, 2011. **71**(7): p. 2550-60.
69. Lee, D.C., et al., *A lactate-induced response to hypoxia.* Cell, 2015. **161**(3): p. 595-609.
70. Hirschhaeuser, F., U.G. Sattler, and W. Mueller-Klieser, *Lactate: a metabolic key player in cancer.* Cancer Res, 2011. **71**(22): p. 6921-5.

71. Goetze, K., et al., *Lactate enhances motility of tumor cells and inhibits monocyte migration and cytokine release.* Int J Oncol, 2011. **39**(2): p. 453-63.
72. Sonveaux, P., et al., *Targeting the lactate transporter MCT1 in endothelial cells inhibits lactate-induced HIF-1 activation and tumor angiogenesis.* PLoS One, 2012. **7**(3): p. e33418.
73. Sutendra, G., et al., *Mitochondrial activation by inhibition of PDKII suppresses HIF1a signaling and angiogenesis in cancer.* Oncogene, 2013. **32**(13): p. 1638-50.
74. Welch, D.R., *Tumor Heterogeneity--A 'Contemporary Concept' Founded on Historical Insights and Predictions.* Cancer Res, 2016. **76**(1): p. 4-6.
75. Heppner, G.H., *Tumor heterogeneity.* Cancer Res, 1984. **44**(6): p. 2259-65.
76. Skibinski, A. and C. Kuperwasser, *The origin of breast tumor heterogeneity.* Oncogene, 2015. **34**(42): p. 5309-16.
77. Huang, S., *Genetic and non-genetic instability in tumor progression: link between the fitness landscape and the epigenetic landscape of cancer cells.* Cancer Metastasis Rev, 2013. **32**(3-4): p. 423-48.
78. Valent, P., et al., *Heterogeneity of neoplastic stem cells: theoretical, functional, and clinical implications.* Cancer Res, 2013. **73**(3): p. 1037-45.
79. Magee, J.A., E. Piskounova, and S.J. Morrison, *Cancer stem cells: impact, heterogeneity, and uncertainty.* Cancer Cell, 2012. **21**(3): p. 283-96.
80. Klein, C.A., *Selection and adaptation during metastatic cancer progression.* Nature, 2013. **501**(7467): p. 365-72.
81. Loeb, L.A., J.H. Bielas, and R.A. Beckman, *Cancers exhibit a mutator phenotype: clinical implications.* Cancer Res, 2008. **68**(10): p. 3551-7; discussion 3557.
82. Loeb, L.A., *Human cancers express mutator phenotypes: origin, consequences and targeting.* Nat Rev Cancer, 2011. **11**(6): p. 450-7.
83. Greaves, M. and C.C. Maley, *Clonal evolution in cancer.* Nature, 2012. **481**(7381): p. 306-13.
84. Nowell, P.C., *The clonal evolution of tumor cell populations.* Science, 1976. **194**(4260): p. 23-8.
85. Merlo, L.M., et al., *Cancer as an evolutionary and ecological process.* Nat Rev Cancer, 2006. **6**(12): p. 924-35.
86. Pepper, J.W., et al., *Cancer research meets evolutionary biology.* Evol Appl, 2009. **2**(1): p. 62-70.
87. Gillies, R.J., D. Verduzco, and R.A. Gatenby, *Evolutionary dynamics of carcinogenesis and why targeted therapy does not work.* Nat Rev Cancer, 2012. **12**(7): p. 487-93.
88. Indraccolo, S., et al., *Interferon-alpha gene therapy by lentiviral vectors contrasts ovarian cancer growth through angiogenesis inhibition.* Hum Gene Ther, 2005. **16**(8): p. 957-70.
89. Favaro, E., et al., *Hypoxia inducible factor-1alpha inactivation unveils a link between tumor cell metabolism and hypoxia-induced cell death.* Am J Pathol, 2008. **173**(4): p. 1186-201.
90. Palorini, R., et al., *Protein Kinase A Activation Promotes Cancer Cell Resistance to Glucose Starvation and Anoikis.* PLoS Genet, 2016. **12**(3): p. e1005931.
91. Bullen, J.W., et al., *Protein kinase A-dependent phosphorylation stimulates the transcriptional activity of hypoxia-inducible factor 1.* Sci Signal, 2016. **9**(430): p. ra56.

http://www.cancer.org/research/cancerfactsstatistics/global

http://emedicine.medscape.com/article/1949171-overview